NASA Contractor Report 187535
ICASE Report No. 91-26

ICASE

UNIFORM HIGH ORDER SPECTRAL METHODS FOR ONE AND TWO DIMENSIONAL EULER EQUATIONS

Wei Cai
Chi-Wang Shu

Contract No. NAS1-18605
March 1991

Institute for Computer Applications in Science and Engineering
NASA Langley Research Center
Hampton, Virginia 23665-5225

Operated by the Universities Space Research Association

National Aeronautics and
Space Administration

Langley Research Center
Hampton, Virginia 23665-5225

UNIFORM HIGH ORDER SPECTRAL METHODS FOR ONE AND TWO DIMENSIONAL EULER EQUATIONS

Wei Cai [1]
Department of Mathematics
University of North Carolina at Charlotte
Charlotte, NC 28223
and
Chi-Wang Shu[2]
Division of Applied Mathematics
Brown University
Providence, RI 02912

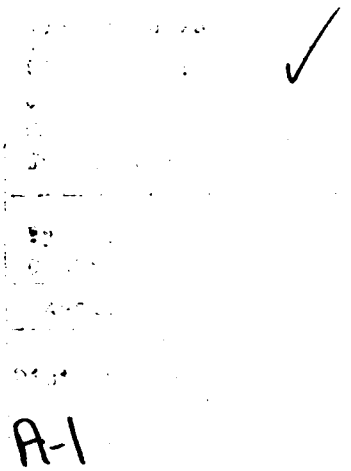

A-1

ABSTRACT

In this paper we study uniform high order spectral methods to solve multi-dimensional Euler equations for gas dynamics. Uniform high order spectral approximations with spectral accuracy in smooth regions of solutions are constructed by introducing the idea of the Essentially Non-Oscillatory (ENO) polynomial interpolations into the spectral methods. Based on the new approximations, we propose nonoscillatory spectral methods which possess the properties of both upwinding difference schemes and spectral methods. We present numerical results for the inviscid Burgers' equation, and for one dimensional Euler equations including the interactions between a shock wave and density disturbance, Sod's and Lax's shock tube problems, and the blast wave problem. Finally, we simulate the interaction between a Mach 3 two dimensional shock wave and a rotating vortex.

[1]Research was supported by NSF grant ASC-9005874, a supercomputing grant from the North Carolina Supercomputer center and a faculty research grant from UNC Charlotte.

[2]Research was supported in part by the National Aeronautics and Space Administration under NASA Contract No. NAS1-18605 while the author was in residence at the Institute for Computer Applications in Science and Engineering (ICASE), NASA Langley Research Center, Hampton, VA 23665. Research was also supported by NSF grant DMS-8810150, NASA Langley grant NAG1-1145, and AFOSR grant 90-0093.

1 Introduction

Recently, high order numerical methods have attracted considerable attentions for the simulation of flows with shock waves and different scales, especially for turbulent flows affected by shock wave interactions. Those high order methods are expected to produce nonoscillatory sharp shock profiles without excessive overall numerical diffusion and, at the same time, be able to resolve the small scales of the flow field elsewhere. Recent results with essentially nonoscillatory (ENO) finite difference methods have shown considerable progress in this direction [9], [17]. Spectral methods, as high order global methods, have been very successful in the study of turbulent flows and flow transition problems when the solutions of the fluid problems are smooth. For those problems, spectral methods have been shown to have an accuracy higher than any algebraic order (so called spectral accuracy) [5]. However it remains to show that spectral methods will also be successful in computing flows with shock waves.

In this paper, we continue our previous work [4] in designing essentially nonoscillatory spectral methods for computing the weak solutions of the hyperbolic system of conservation laws

$$\mathbf{u}_t + \mathbf{f}(\mathbf{u})_x + \mathbf{g}(\mathbf{u})_y = 0 \tag{1.1}$$

$$\mathbf{u}(x, y, 0) = \mathbf{u}_0(x, y). \tag{1.2}$$

Here, as usual, $\mathbf{u} = (u_1, \cdots, u_s)^T$ is a state vector and $\mathbf{f}(\mathbf{u}), \mathbf{g}(\mathbf{u})$ are the vector-valued flux functions of s components. The system is assumed to be hyperbolic in the sense that for any real vector $\xi = (\xi_1, \xi_2)$, the matrix $\xi_1 \frac{\partial \mathbf{f}}{\partial \mathbf{u}} + \xi_2 \frac{\partial \mathbf{g}}{\partial \mathbf{u}}$ always has s - real eigenvalues and a complete set of eigenvectors. The solutions to (1.1) usually develop discontinuities in the form of shock waves and contact discontinuities.

In applying spectral methods to problems having discontinuous solutions, a key issue is how to deal with the Gibbs phenomenon caused by the discontinuities of the solutions. The overall accuracy of spectral methods will be, at most, first order everywhere in the presence of Gibbs oscillations. There are various filtering techniques to recover spectral accuracy in regions away from the discontinuities [8], [14]. On the other hand, one-sided filtering can be used to obtain uniform convergence in regions close to the discontinuities[2]. As another approach to treat the Gibbs oscillation, in [4] we proposed a nonoscillatory spectral approximation to discontinuous solutions by adding piecewise linear functions, such as sawtooth-like functions and step functions, to the conventional Fourier trigonometric or Chebyshev polynomial spaces. Those additional functions are used to resolve the discontinuities in the

solutions caused by shock waves and contact discontinuities. The cell-averaged form of (1.1) is used to formulate the numerical schemes, resulting in Godunov-type shock capturing algorithms. The usual reconstruction step between cell averages and point values of the numerical solutions in such schemes can be performed efficiently with Fast Fourier Transforms. However, a common problem with cell-averaged formulation is the costly implementation of the reconstruction in multi-dimensional problems.

In this paper, we adopt the same philosophy as in [4], however, a more robust and sophisticated technique will be introduced. With the new technique, we will be able to achieve global convergence up to any given m-th order ($m > 0$) and , meanwhile, retain spectral accuracy in the regions away from the discontinuities. In order to achieve these goals, we incorporate the main idea of the ENO polynomial interpolations [9] into our construction of uniform spectral approximations. We also introduce the idea of upwind differencing from conservative finite difference methods into the design of the spectral schemes. The idea of upwinding has proven very successful in capturing shock wave fronts and producing the right entropy solutions. By using local Riemann solvers and flux limiters, modern shock capturing finite difference schemes, such as the TVD schemes [9] , MUSCL type schemes [19], FCT schemes [1], and the more recent ENO schemes [9] [17], produce very satisfactory shock profiles and entropy satisfying solutions. The nonoscillatory spectral approximations proposed in this paper will enable us to bring the upwinding idea into the framework of spectral methods. Meanwhile, the spectral schemes will be based directly on the conservation laws (1.1), not on its cell-averaged form. Thus, generalization to multi-dimensional cases is straightforward.

For systems of conservation laws, in order to achieve sharp shock profile without spurious oscillations, numerical flux operators for the scalar equations are usually applied to the locally defined characteristic variables. Because of this complication, it has been realized that the cost of upwinding schemes is much greater than that of the centered difference schemes. Several attempts have been made to eliminate this shortcoming by combining centered difference schemes and upwinding schemes. In [13], a mixed method of centered difference schemes and ENO schemes was studied and, in [6], the authors suggested a type of nonlinear filtering technique to modify the results of the Lax-Wendroff scheme at each time step to produce nonoscillatory TVD solutions. Even though it is achieved in a quite different way from those in [6] and [13], the result in this paper will provide another example of blending the nice properties of both upwinding schemes and centered difference schemes (in this case, spectral schemes).

This paper is organized as follows: in Section 2, we first briefly review the method proposed in [4], then present the new method of constructing uniform convergent, up to any

given m-th order($m > 0$), spectral approximations to discontinuous functions. In Section 3, we study the nonoscillatory spectral methods for scalar conservation laws. Extensions to the system of conservation laws and multi-dimensional problems will be discussed in Section 4. In Section 5, we present numerical experiments for the new methods. First, the uniform convergence and the spectral accuracy of the proposed spectral approximations are tested on discontinuous functions. Then we study the global accuracy of the spectral schemes on a scalar inviscid Burgers' equation and on one dimensional Euler equations which model the interaction of a pure shock wave with density waves. Also we apply the scheme to the standard Sod's and Lax's test problems [16] in order to check the convergence of our spectral schemes to the correct entropy solutions. High order numerical results will also be presented for solving the interaction between two blast waves [20]. Finally we apply the spectral schemes to simulate the interactions between a Mach 3 two-dimensional shock wave and a rotating vortex.

2 Uniform High Order Spectral Approximations

The conventional Fourier spectral space has basis functions $\{e^{ikx}\}_{|k|\le N}$. The Fourier expansions for discontinuous functions converge very slowly. For instance, consider a sawtooth-like function

$$F(x, x_s, A) = A \begin{cases} -x & \text{for } x \le x_s, \\ 2\pi - x & \text{for } x > x_s, \end{cases} \tag{2.1}$$

where x_s is the location of the discontinuity and $A = \frac{F(x_s^+) - F(x_s^-)}{2\pi} = [F]_{x_s}$ is the jump of $F(x, x_s, A)$ across x_s. The partial sum of the Fourier expansion of $F(x, x_s, A)$ is

$$F_N(x, x_s, A) = \sum_{|k|\le N} \hat{f}_k(x_s, A) e^{ikx}, \tag{2.2}$$

where

$$\hat{f}_k(x_s, A) = \frac{1}{2\pi} \int_0^{2\pi} F(x, x_s, A) e^{-ikx}\, dx = A \begin{cases} \frac{e^{-ikx_s}}{ik} & \text{for } |k| \ge 1, \\ (\pi - x_s) & \text{for } k = 0. \end{cases} \tag{2.3}$$

From (2.3) we can see that the Fourier coefficients $\hat{f}_k(x_s, A)$ only decay like $O(\frac{1}{k})$ as $k \to \infty$. As a result, the convergence of (2.2) will be only first order, and moreover, the Gibbs oscillations near x_s will be in the order of $O(1)$. In order to get rid of the Gibbs oscillations, in [4] we proposed a technique to construct essentially nonoscillatory spectral approximations, which we review below.

Let $u(x)$ be a piecewise C^∞ periodic function with a jump discontinuity at x_s with jump $[u]_{x_s}$ and let $u_N(x)$ be its finite Fourier expansion, the nonoscillatory spectral approximation is defined by

$$u_N^*(x) = \sum_{|k|\le N} a_k e^{ikx} + \sum_{|k|>N} \frac{A'}{ik} e^{-iky} e^{ikx}, \tag{2.4}$$

where y is an approximation of x_s and A' is an approximation of $[u]_{x_s}$ and

$$a_k = \frac{1}{2\pi} \int_0^{2\pi} u(x) e^{-ikx}\, dx.$$

Since the second sum in (2.4) is actually $F(x,y,A') - F_N(x,y,A')$, we have

$$u_N^*(x) = \sum_{|k|\le N} [a_k - \hat{f}_k(y,A')] e^{ikx} + F(x,y,A'). \tag{2.5}$$

Therefore $u_N^*(x)$ defines an approximation in the spectral space $\{e^{ikx}\}_{|k|\le N}$ augmented by sawtooth-like functions $F(x,y,A')$.

The approximation defined in (2.5) yields nonoscillatory numerical results for discontinuous functions, and spectral schemes using this approximation have given high order accuracy for one-dimensional Euler gas dynamics equations ([2], [3]). In order for (2.5) to be nonoscillatory, the approximation for the location and the magnitude of the shock should be reasonably accurate. Second order accuracy in the location and first order accuracy in the magnitude are needed to ensure the uniform nonoscillatory convergence.

In what follows, we present a different method which will be uniformly convergent up to any given order $m > 0$ and , at the same time, retain the spectral accuracy in the smooth regions away from the discontinuities. Furthermore, the requirement of accuracy in shock locations will be much relaxed and an approximation to the magnitude of the shock is not needed. This makes the computation more robust.

Before we discuss the new approximation method we review two techniques to be used in our construction. The first one is the essentially non-oscillatory (ENO) polynomial interpolation, and the second is the filtering technique for Fourier approximations.

ENO Polynomial Interpolation

We will follow the notation used in [9]. Let $u(x)$ be a function defined on $I = [0, 2\pi]$ and $\{x_i\}_{i=0}^N$ be the uniform mesh on I, $x_i = ih, h = \frac{2\pi}{N}$. For simplicity of illustration, we assume that $u(x)$ has only one discontinuity at $x_s \in I$. Now given $u(x_i)$, $0 \le i \le N$, define a piecewise m-th order polynomial interpolant $Q_m(x;u)$ for $u(x)$ at mesh points x_i, $0 \le i \le N$ as follows:

$$Q_m(x_i;u) = u(x_i) \qquad \text{for } 0 \le i \le N, \tag{2.6}$$

and

$$Q_m(x;u) = q_{m,j+\frac{1}{2}}(x;u) \qquad \text{for } x_j \le x \le x_{j+1}, \tag{2.7}$$

where $q_{m,j+\frac{1}{2}}(x;u)$ is a polynomial of degree m defined below.

Polynomial $q_{m,j+\frac{1}{2}}(x;u)$ interpolates $u(x)$ at $(m+1)$ successive points x_i, $i_m(j) \leq i \leq i_m(j)+m$. The stencil of these $(m+1)$ mesh points will be chosen according to the smoothness of the data $u(x_i)$ around x_j. A recursive algorithm to define $i_m(j)$ starts by defining

$$i_1(j) = j \tag{2.8}$$

i.e. $q_{1,j+\frac{1}{2}}(x)$ will be the first degree polynomial which interpolates $u(x)$ at x_j, x_{j+1}. If we assume $q_{k,j+\frac{1}{2}}(x)$ is the k - th degree polynomial which interpolates $u(x)$ at

$$x_{i_k(j)}, \cdots, x_{i_k(j)+k}, \tag{2.9}$$

then we need one additional mesh point in order to define $q_{k+1,j+\frac{1}{2}}(x)$. That point may be the nearest one to the left of stencil of (2.9) (i.e. $x_{i_k(j)-1}$) or the nearest one to the right of the stencil of (2.9) (i.e. $x_{i_k(j)+k+1}$). The choice will be based on the absolute values of the corresponding $(k+1)$-th order divided differences, namely

$$i_{k+1}(j) = \begin{cases} i_k(j)-1 & \text{if } u[x_{i_k(j)-1}, \cdots, x_{i_k(j)+k}] < u[x_{i_k(j)}, \cdots, x_{i_k(j)+k+1}], \\ i_k(j) & \text{otherwise.} \end{cases} \tag{2.10}$$

The piecewise polynomial $Q_m(x;u)$ defined in (2.6), (2.7) will give uniform nonoscillatory approximations to $u(x)$ up to the discontinuities. In fact it can be shown that

$$\frac{d^k}{dx^k}Q_m(x;u) = \frac{d^k}{dx^k}u(x) + O(h^{m+1-k}) \qquad \text{for } 0 \leq k \leq m. \tag{2.11}$$

except for the cell containing x_s. Using sub-cell resolutions [10] this is also correct in the shocked cell.

Filtering Techniques for Fourier Approximations

When a function $u(x)$ is discontinuous, its Fourier approximation $u_N(x)$ will be at most first order everywhere [7] . However, there are several ways to recover the loss of the spectral accuracy in the smooth regions of the function $u(x)$ ([8], [14]). The most common way is to multiply the Fourier coefficients of $u(x)$ by a decreasing scalar factor σ_k. $|\sigma_k| \to 0$ as $|k| \to N$. Then the resulting series (the filtered approximation) will be denoted by $u_N^\sigma(x)$,

$$u_N^\sigma(x) = \sum_{|k|\leq N} \sigma_k a_k e^{ikx}. \tag{2.12}$$

It was proven in [20] that, if σ_k is derived from a scalar function $\sigma(t), 0 \leq t \leq 1$ and $\sigma_k = \sigma(\frac{|k|}{N}), |k| \leq N$, and $\sigma(t)$ satisfies the following conditions:

$$\begin{aligned} \sigma(0) &= 1, \\ \sigma(1) &= 0, \\ \sigma^{(k)}(0) = \sigma^{(k)}(1) &= 0 \qquad \text{for } 1 \le k \le K, \end{aligned} \tag{2.13}$$

then $u_N^\sigma(x)$ will converge to $u(x)$ in the smooth regions of $u(x)$ in the order of $O(\frac{1}{N^{K+1}})$. In the actual computations, σ_k is chosen to decay exponentially in terms of the frequency number,

$$\sigma_k = e^{-\alpha(\frac{k}{N})^{2\ell}} \qquad \text{for } |k| \le N, \tag{2.14}$$

where the constant α is chosen so that σ_N is the machine zero and 2ℓ is called the order of the exponential filtering.

Uniform Spectral Approximations

Now we present our new uniform high order nonoscillatory spectral approximations to discontinuous functions. Again, for simplicity, we assume $u(x)$ is a periodic piecewise C^∞ function on $[0, 2\pi]$ with only one discontinuity at x_s. Also we assume that the discontinuity has been detected within an interval $[x_s^l, x_s^r]$.

Let us denote all the mesh points inside interval $[x_s^l, x_s^r]$ as $x_{i_l}, \cdots, x_{i_r}$. Then we define a piecewise m - th order polynomial $\varphi(x)$ which interpolates the function $u(x)$ at mesh points x_i, $i_l \le i \le i_r$,

$$\varphi(x) = \begin{cases} q_{m,j+\frac{1}{2}}(x) & \text{if } x \in [x_j, x_{j+1}] \cap [x_s^l, x_s^r] \text{ for some } j, \\ P_l(x) & \text{if } x \in [0, x_s^l], \\ P_r(x) & \text{if } x \in [x_s^r, 2\pi], \end{cases} \tag{2.15}$$

where $q_{m,j+\frac{1}{2}}(x)$ was defined in (2.8) - (2.10) and $P_l(x)$ and $P_r(x)$ are both m'-th order polynomials on the interval $[0, x_s^l]$ and $[x_s^r, 2\pi]$ respectively , $m' = 2m + 1$, and satisfy the following conditions,

$$\begin{aligned} P_l^{(k)}(x_s^l) &= q_{m,i_l-\frac{1}{2}}^{(k)}(x_s^l), \\ & \qquad\qquad \text{for } 0 \le k \le m \\ P_r^{(k)}(x_s^r) &= q_{m,i_r+\frac{1}{2}}^{(k)}(x_s^r), \end{aligned} \tag{2.16}$$

and

$$\begin{aligned} P_l^{(k)}(x_s^r - 2\pi) &= q_{m,i_r+\frac{1}{2}}^{(k)}(x_s^r), \\ & \qquad\qquad \text{for } 0 \le k \le m \\ P_r^{(k)}(x_s^l + 2\pi) &= q_{m,i_l-\frac{1}{2}}^{(k)}(x_s^l). \end{aligned} \tag{2.17}$$

Conditions (2.16) (2.17) ensure that $\varphi(x)$ will be at least globally C^m continuous. There are exact $2m+2 = m'+1$ constraints on the m'-th polynomials $P_l(x)$ and $P_r(x)$ respectively. Therefore they are uniquely defined. By (2.11), the function $\varphi(x)$ will have the following property,

$$\begin{aligned} \varphi(x_i) &= u(x_i) \qquad \text{for } i_l \le i \le i_r, & (2.18)\\ \varphi(x) - u(x) &= O(h^{m+1}) \qquad \text{for } x \in [x_s^l, x_s^r]. & (2.19) \end{aligned}$$

Next we consider the difference between $u(x)$ and $\varphi(x)$, $v(x) = u(x) - \varphi(x)$. $v(x)$ will be a C^m function everywhere in $[0, 2\pi]$ except at x_s where $[v(x)]_{x_s} = O(h^{m+1})$. Moreover, $v(x_i) = 0$, $i_l \le i \le i_r$. Therefore, the filtered Fourier interpolant $I_N^\sigma v(x)$ will converge to $v(x)$ rapidly,

$$\begin{aligned} v_N^\sigma(x) = I_N^\sigma v(x) &= \sum_{k=-\frac{N}{2}}^{\frac{N}{2}-1} \sigma_k \hat{v}_k e^{ikx},\\ \hat{v}_k &= \frac{1}{N}\sum_{i=0}^{N}(v(x_i) - \varphi(x_i))e^{-ikx_i}\\ &= \frac{1}{N}\sum_{i<i_l}(u(x_i) - P_l(x_i))e^{-ikx_i} + \frac{1}{N}\sum_{i>i_r}(u(x_i) - P_r(x_i))e^{-ikx_i}, \end{aligned}$$

and σ_k is the filter in (2.14).

Finally we define the uniform spectral approximation $\mathcal{P}u(x)$ of $u(x)$ by

$$\mathcal{P}u(x) = \varphi(x) + v_N^\sigma(x), \qquad \text{for } x \in [0, 2\pi]. \tag{2.20}$$

Then the derivatives of $u(x)$ will be approximated by those of $\mathcal{P}u(x)$, i.e.

$$\frac{d^k}{dx^k}u(x) \sim \frac{d^k}{dx^k}\mathcal{P}u(x) \qquad \text{for } k > 0. \tag{2.21}$$

To see the accuracy of (2.20) to $u(x)$, let $\rho(x) \in C_0^\infty(x_s^l, x_s^r)$ be a mollifier function such that

$$\rho(x) = 1 \qquad \text{for } x \text{ near } x_s, \tag{2.22}$$

and

$$v^*(x) = \begin{cases} \rho(x)v(x) & \text{if } x \in [x_s^l, x_s^r],\\ v(x) & \text{otherwise.} \end{cases} \tag{2.23}$$

One can easily see that

$$v^*(x_i) = v(x_i) \qquad \text{for } 0 \le i \le N, \tag{2.24}$$

and hence

$$I_N v^*(x) = I_N v(x). \tag{2.25}$$

As $v^*(x) \in C^m(0, 2\pi)$ and is periodic, by standard estimate it can be shown [2] that

$$\|v^*(x) - I_N^\sigma v^*(x)\|_{L_2} \le c\frac{\|v^{*(m)}\|_{L_2}}{N^{m+1}}, \tag{2.26}$$

where c is a constant independent of N.

On the other hand,

$$\begin{aligned} \|v^*(x) - v(x)\|_{L_2} &= \sqrt{\int_{x_s^l}^{x_s^r} (1-\rho(x))^2 v^2(x)\,dx} \\ &\le \sqrt{\int_{x_s^l}^{x_s^r} v^2(x)\,dx} \\ &\le \sqrt{\int_{x_s^l}^{x_s^r} (u(x)-\varphi(x))^2\,dx}, \end{aligned} \tag{2.27}$$

by (2.19) we have

$$\|v^*(x) - v(x)\|_{L_2} = O(h^{m+1}). \tag{2.28}$$

It follows from (2.26) and (2.28) that

$$\begin{aligned} & \|v(x) - I_N^\sigma v(x)\|_{L_2} = \|v(x) - I_N^\sigma v^*(x)\|_{L_2} \\ \le\ & \|v(x) - v^*(x)\|_{L_2} + \|v^*(x) - I_N^\sigma v^*(x)\|_{L_2} \\ =\ & O(h^{m+1}). \end{aligned} \tag{2.29}$$

Thus

$$\begin{aligned} \|\mathcal{P}u(x) - u(x)\|_{L_2} &= \|[\varphi(x) + I_N^\sigma v(x)] - [\varphi(x) + v(x)]\|_{L_2} \\ &= \|v(x) - I_N^\sigma(x)\|_{L_2} = O(h^{m+1}), \end{aligned} \tag{2.30}$$

which establishes the uniform $(m+1)$-th order convergence of the approximation $\mathcal{P}u$ of u in the L_2 norm. Error estimates in a higher order Sobolev norm can be derived similarly.

The spectral convergence of $\mathcal{P}u(x)$ to $u(x)$ in the regions outside $[x_s^l, x_s^r]$ follows from the spectral convergence of $v_N^\sigma(x)$ to $v(x)$ in the smooth regions of $v(x)$.

3 Uniform High Order Spectral Methods

In this section we study uniform high order spectral methods for conservations laws (1.1). First, we will consider the scalar one-dimensional conservation laws. Extensions to the

system of conservation laws and to multi-dimensional problems will be discussed in Section 4.

We will derive the spectral schemes using the method of lines. The time derivative and spatial derivatives will be discretized separately. For simplicity we only present the Euler-forward difference method for the time derivative. In the numerical experiments of Section 5 a high order TVD type Runge-Kutta time discretization [17] is used. The numerical scheme will be written in the following conservative form,

$$u_j^{n+1} = u_j^n - \lambda(\hat{f}_{j+\frac{1}{2}} - \hat{f}_{j-\frac{1}{2}}), \tag{3.1}$$

where $u_j^n \sim u(x_j, t_n), x_j = j\Delta x, t_n = n\Delta t$, and Δx and Δt are the spatial mesh size and the time step respectively, $\lambda = \frac{\Delta t}{\Delta x}$, $\hat{f}_{j+\frac{1}{2}}$ are the numerical fluxes .

It is observed [17] that if there is a function $h(x)$ such that

$$f(u(x)) = \frac{1}{\Delta x}\int_{x-\frac{\Delta x}{2}}^{x+\frac{\Delta x}{2}} h(\xi)\,d\xi, \tag{3.2}$$

then

$$f_x(u(x_j)) = \frac{h(x_{j+\frac{1}{2}}) - h(x_{j-\frac{1}{2}})}{\Delta x}. \tag{3.3}$$

This suggests that the numerical flux $\hat{f}_{j+\frac{1}{2}}$ should approximate $h(x_{j+\frac{1}{2}})$ as $\Delta x \to 0$.

We construct $h(x)$ in the same manner as in [17] via its primitive function $H(x)$ modulo a linear function,

$$H(x) = \int_{-\frac{\Delta x}{2}}^{x} (h(\xi) - c)\,d\xi, \tag{3.4}$$

where c is a constant chosen so that $H(x)$ will be a periodic function:

$$c = \int_{-\frac{\Delta x}{2}}^{2\pi-\frac{\Delta x}{2}} h(\xi)\,d\xi = \Delta x \sum_{j=0}^{N-1} f_j. \tag{3.5}$$

Assuming that (3.2) holds, then

$$\begin{aligned} H(x_{j+\frac{1}{2}}) &= \int_{-\frac{\Delta x}{2}}^{x_{j+\frac{1}{2}}} (h(\xi) - c)\,d\xi \\ &= \sum_{k=0}^{j} \int_{x_{k-\frac{1}{2}}}^{x_{k+\frac{1}{2}}} h(\xi)\,d\xi - c(j+1)\Delta x \\ &= \Delta x \sum_{k=0}^{j} f(u(x_k)) - c(j+1)\Delta x \qquad \text{for } 0 \le j \le N. \end{aligned} \tag{3.6}$$

We then form the uniform spectral approximation operator $\mathcal{P}H$ to $H(x)$,

$$\mathcal{P}H = \varphi(x) + v_N^{\sigma}(x), \tag{3.7}$$

where $\varphi(x)$ is the piecewise m-th polynomial defined in (2.15) and $v_N^\sigma(x)$ is the filtered Fourier interpolant of data $H(x_{j+\frac{1}{2}}) - \varphi(x_{j+\frac{1}{2}})$, $0 \le j \le N$. As before, it is assumed that the shock discontinuity or contact discontinuity x_s (for simplicity of illustration, only one such discontinuity is assumed to exist) has been detected in an interval $[x_s^l, x_s^r]$, i.e.

$$x_s \in [x_s^l, x_s^r]. \tag{3.8}$$

If $x \in [x_j, x_{j+1}] \cap [x_s^l, x_s^r]$ for some j, $\varphi(x) = q_{m,j+\frac{1}{2}}(x)$. $q_{m,j+\frac{1}{2}}(x)$ is a m-th order polynomial and

$$q_{m,j+\frac{1}{2}}(x_{i+\frac{1}{2}}) = H(x_{i+\frac{1}{2}}) \qquad \text{for } i_m(j) \le i \le i_m(j) + m. \tag{3.9}$$

The stencil $i_m(j), \cdots, i_m(j) + m$ is defined recursively as in (2.8) - (2.10), however the first point of the stencil $i_1(j)$ is chosen according to the local Roe-speed $a_{j+\frac{1}{2}}$,

$$a_{j+\frac{1}{2}} = \frac{f(u_{j+1}) - f(u_j)}{u_{j+1} - u_j}, \tag{3.10}$$

i.e.

$$i_1(j) = \begin{cases} j, & \text{if } a_{j+\frac{1}{2}} \ge 0, \\ j+1, & \text{if } a_{j+\frac{1}{2}} < 0. \end{cases} \tag{3.11}$$

Then we have the following spectral algorithm

Algorithm I (Spectral ENO-Roe)

- Step 1, define $H(x_{j+\frac{1}{2}}), 0 \le j \le N$ by (3.6) and their uniform spectral approximation $\mathcal{P}H(x)$ by (3.7);
- Step 2, let

$$\hat{f}_{j+\frac{1}{2}} = \frac{d}{dx}\mathcal{P}H(x_{j+\frac{1}{2}}) + c = \frac{d}{dx}\varphi(x_{j+\frac{1}{2}}) + \frac{d}{dx}v_N^\sigma(x_{j+\frac{1}{2}}) + c, \tag{3.12}$$

  where constant c is defined in (3.5).

Remarks

1. The evaluation of $\frac{d}{dx}v_N^\sigma(x_{j+\frac{1}{2}}), 0 \le j \le N$ can be performed efficiently via the Fast Fourier Transforms with the total number of operations of order $O(N \log N)$;
2. Regarding the first term, $\frac{d}{dx}\varphi(x_{j+\frac{1}{2}}), 0 \le j \le N$, only for those $x_{j+\frac{1}{2}} \in [x_s^l, x_s^r]$, do we need to do the ENO interpolation and the numerical differentiation. If $x_{j+\frac{1}{2}}$ is located outside $[x_s^l, x_s^r]$, the derivatives can be computed analytically without additional computer cost;

3. The formal spatial accuracy of **Algorithm I** will be spectrally accurate in the smooth regions of the solution and uniformly m-order elsewhere;

4. (Entropy Correction) the fluxes $\hat{f}_{j+\frac{1}{2}}$ defined in (3.12) are based on the Roe flux which admits "expansion shocks". We use an entropy correction discussed in [17], see also Harten [11] for the origination of such corrections.

4 Euler Equations of Gas Dynamics

In this section we extend the scalar **Algorithm I** from the previous section to the system of Euler equations for gas dynamics for polytropic gas. With all variables in bold face denoting vectors, we have the following Euler equations:

$$\begin{aligned} \mathbf{u}_t &+ \mathbf{f}(\mathbf{u})_x = 0, && (4.1)\\ \mathbf{u} &= (\rho, m, E)^\top, && (4.2)\\ \mathbf{f}(\mathbf{u}) &= q\mathbf{u} + (0, P, qP)^\top, && (4.3)\\ P &= (\gamma - 1)(E - \frac{1}{2}\rho q^2). && (4.4) \end{aligned}$$

Here ρ, q, P and E are the density, velocity, pressure and total energy respectively, $m = \rho q$ is the momentum and $\gamma = 1.4$ is the ratio of specific heats of a polytropic gas.

The eigenvalues of the Jacobian matrix $\mathbf{A}(\mathbf{u}) = \frac{\partial \mathbf{f}}{\partial \mathbf{u}}$ are

$$\lambda_1(\mathbf{u}) = q - c,\ \lambda_2(\mathbf{u}) = q,\ \lambda_3(\mathbf{u}) = q + c, \tag{4.5}$$

where $c = (\gamma P/\rho)^{\frac{1}{2}}$ is the sound speed.

The corresponding right-eigenvectors are

$$\mathbf{r}_1(\mathbf{u}) = \begin{pmatrix} 1 \\ q - c \\ H - qc \end{pmatrix}, \mathbf{r}_2(\mathbf{u}) = \begin{pmatrix} 1 \\ q \\ \frac{1}{2}q^2 \end{pmatrix}, \mathbf{r}_3(\mathbf{u}) = \begin{pmatrix} 1 \\ q + c \\ H + qc \end{pmatrix}, \tag{4.6}$$

where

$$H = (E + P)/\rho = c^2/(\gamma - 1) + \frac{1}{2}q^2,$$

is the enthalpy.

The corresponding left eigenvectors $\{\mathbf{l}_k(\mathbf{u})\}$ which are bi-orthonormal to $\{\mathbf{r}_k(\mathbf{u})\}$ in (4.6) are

$$\begin{aligned} \mathbf{l}_1(\mathbf{u}) &= \frac{1}{2}(b_2 + q/c, -b_1 q - 1/c, b_1),\\ \mathbf{l}_2(\mathbf{u}) &= (1 - b_2, b_1 q, -b_1), && (4.7)\\ \mathbf{l}_3(\mathbf{u}) &= \frac{1}{2}(b_2 - q/c, -b_1 q + 1/c, b_1), \end{aligned}$$

where

$$b_1 = (\gamma - 1)/c^2, \tag{4.8}$$

$$b_2 = \frac{1}{2} q^2 b_1. \tag{4.9}$$

As in the case of scalar conservation laws, we first define a vector counterpart $\mathbf{H}(x_{j+\frac{1}{2}})$, $0 \le j \le N$ of (3.6). The scalar quantities $f(u(x_k))$ in (3.6) are replaced by the vectors $\mathbf{f}(\mathbf{u}(x_k))$. We then generalize the construction of the uniform spectral approximation operator $\mathcal{P}\mathbf{H}$ to vector-valued functions in the following way. As before, the assumption about the shock location (3.8) still holds here. We have the uniform spectral approximation

$$\mathcal{P}\mathbf{H}(x) = \mathbf{\Phi}(x) + \mathbf{v}_N^{\sigma}(x), \tag{4.10}$$

where the components of the vector-valued function $\mathbf{\Phi}(x)$ will be piecewise m-th order polynomials and $\mathbf{v}_N^{\sigma}(x)$ will be the filtered Fourier interpolant of vector quantities $\mathbf{H}(x_{j+\frac{1}{2}}) - \mathbf{\Phi}(x_{j+\frac{1}{2}}), 0 \le j \le N$.

$\mathbf{\Phi}(x)$ will be defined separately according to whether x is inside or outside the interval $[x_s^l, x_s^r]$. For $x \in [x_j, x_{j+1}] \cap [x_s^l, x_s^r]$ for some j, first let $q_{m,j+\frac{1}{2}}^{(k)}(x)$ be the ENO polynomial interpolant of the characteristic variables $\mathbf{H}^{(k)}(x_{i+\frac{1}{2}}), j - m \le i \le j + m$. Here as usual the characteristic variables $\mathbf{H}^{(k)}(x_{i+\frac{1}{2}})$ are the projections of $\mathbf{H}(x_{i+\frac{1}{2}})$ on the locally defined characteristic fields. In this paper, we define the local characteristic fields with respect to the Roe-averaged state $\bar{\mathbf{u}}_{j+\frac{1}{2}}$ between the states $\mathbf{u}_j, \mathbf{u}_{j+1}$, i.e.

$$\mathbf{H}^{(k)}(x_{i+\frac{1}{2}}) = \mathbf{l}_k(\bar{\mathbf{u}}_{j+\frac{1}{2}})\mathbf{H}(x_{i+\frac{1}{2}}) \tag{4.11}$$

for $j - m \le i \le j + m, 1 \le k \le 3$. See [15] for the definition of $\bar{\mathbf{u}}_{j+\frac{1}{2}}$.

We thus have

$$q_{m,j+\frac{1}{2}}^{(k)}(x_{i+\frac{1}{2}}) = \mathbf{H}^{(k)}(x_{i+\frac{1}{2}}) \qquad \text{for } i_m(j) \le i \le i_m(j) + m. \tag{4.12}$$

and, in the recursive process of choosing the stencil $i_m(j)$, the first point $i_1(j)$ is determined according to the sign of the local eigenvalue:

$$i_1(j) = \begin{cases} j & \text{if } \lambda^{(k)}(\bar{\mathbf{u}}_{j+\frac{1}{2}}) \ge 0, \\ j+1 & \text{if } \lambda^{(k)}(\bar{\mathbf{u}}_{j+\frac{1}{2}}) < 0. \end{cases} \tag{4.13}$$

We then define the vector-valued function $\mathbf{\Phi}(x)$ as

$$\mathbf{\Phi}(x) = \sum_{k=1}^{3} q_{m,j+\frac{1}{2}}^{(k)}(x)\mathbf{r}_k(\bar{\mathbf{u}}_{j+\frac{1}{2}}) \qquad \text{for } x \in [x_j, x_{j+1}]. \tag{4.14}$$

On the other hand, when x is outside of the interval $[x_s^l, x_s^r]$, we define $\mathbf{\Phi}(x)$ in the same way as in (2.16) and (2.17). Therefore, in those regions the components of $\mathbf{\Phi}(x)$ will be $m' = 2m + 1$-th order polynomials. Globally, the components of $\mathbf{\Phi}(x)$ will be C^m function for $x \in [0, 2\pi]$ and

$$\mathbf{\Phi}(x_{i+\frac{1}{2}}) = \mathbf{H}(x_{i+\frac{1}{2}}), \qquad \text{if } x_{i+\frac{1}{2}} \in [x_s^l, x_s^r]. \tag{4.15}$$

Now we present our algorithm for (4.1)

Algorithm II (Spectral-ENO-Roe)

- Step 1, define vector quantities $\mathbf{H}(x_{j+\frac{1}{2}}), 0 \le j \le N$ by (3.6) and their uniform spectral approximation $\mathcal{P}\mathbf{H}(x)$ by (4.10);
- Step 2, let

$$\hat{\mathbf{f}}_{j+\frac{1}{2}} = \frac{d}{dx}\mathcal{P}\mathbf{H}(x_{j+\frac{1}{2}}) + c = \frac{d}{dx}\mathbf{\Phi}(x_{j+\frac{1}{2}}) + \frac{d}{dx}\mathbf{v}_N^{\sigma}(x_{j+\frac{1}{2}}) + c, \tag{4.16}$$

where c is defined as in (3.5) with f_j replaced by $\mathbf{f}_j$.

Remarks

1. All of the remarks following **Algorithm I** of the previous section apply to **Algorithm II**. However, the entropy correction is used only on the genuine nonlinear fields. The total number of operations in the computations of all $\hat{\mathbf{f}}_{j+\frac{1}{2}}, 0 \le j \le N$ will be of order $O(N \log N)$. Moreover, the characteristic decompositions are only needed for those $x_{j+\frac{1}{2}}$ in $[x_s^l, x_s^r]$ where a shock discontinuity or contact discontinuity has been detected;
2. (Generalization to Mulit-dimensional Cases) For the system of conservation laws in two dimensions (1.1), we apply **Algorithm II** to $\mathbf{f}(\mathbf{u})$ and $\mathbf{g}(\mathbf{u})$ separately. Characteristic decompositions will be performed on their corresponding characteristic fields when needed. The same idea can be applied to higher dimensional cases.

5 Numerical Results

In this section, we will carry out several numerical experiments with **Algorithm I & II**. In implementing these algorithms, we have to choose the order of ENO interpolations in (3.7) or (4.10) and the interval $[x_s^l, x_s^r]$ as defined in (3.8), which is detected to contain a shock or contact discontinuity. In most of the tests, we choose third order ENO interpolation, i.e. $m = 3$, unless it is mentioned otherwise. The interval $[x_s^l, x_s^r]$ is usually chosen to contain 6 - 8 mesh points around a discontinuity. The numerical results show insensitivity to the size of $[x_s^l, x_s^r]$ as long as it contains all the transition points in the numerical shock. To detect the shock we have used the basic check on the gradients of the numerical data. Define

$$t_j = max(|u(j) - u(j-1)|, |u(j+1) - u(j)|) \tag{5.1}$$

If $t_j > max(3.0t_{j-2}, 3.0t_{j+2}, \alpha)$, where α is chosen dynamically according to the structure of the shock wave, then we decide that the interval $[x_{j-1}, x_{j+1}]$ contains a discontinuity. Because of the global high order of the scheme, a falsely detected shock location in a smooth region of the solution would not destroy the overall accuracy of the scheme.

To retain the spectral accuracy in the smooth region of the solutions, we apply high order exponential cut-off filters in (2.14). It is our experience that a very weak filter (i.e. high order) will suffice to get high accuracy in the smooth region.

Time Discretization for Chebyshev Methods

The time derivative in (4.1) is discretized with the Runge-Kutta method. We have used the third order Runge-Kutta method proposed in [17] which yields TVD (total variation vanishing) results if the spatial discretization is TVD.

For periodical problems, the spatial derivative is approximated by Fourier trigonometric polynomials. When the solution is nonperodic, Chebyshev polynomials are used instead. A common difficulty, however, with Chebyshev methods is the stringent time step restriction. In general, the time step Δt has to be in the order of $O(\frac{1}{N^2})$ where N is the order of the Chebyshev polynomials. This is a direct consequence of the clustering of Chebyshev collocation points near both boundaries. For many hyperbolic problems, this dense distribution of mesh points near boundaries is not necessary, as for most of the test problems in this paper. Recently in [12], a novel mesh transformation is proposed to relax the restriction of the Chebyshev methods on time steps. If x denotes the physical coordinate and ξ the computational coordinate, the following transformation is considered in [12] :

$$\xi = \frac{\sin^{-1} \alpha x}{\sin^{-1} \alpha} \qquad |x| \leq 1, |\xi| \leq 1. \tag{5.2}$$

If $\xi_i = \cos i\frac{\pi}{N}, 0 \leq i \leq N$ is the Chebyshev mesh in the $\xi-$space, then $x_i = \frac{1}{\alpha}\sin(\sin^{-1}\alpha\xi_i)$ will be the corresponding mesh in the $x-$space. Because of the stretching nature of the transformation (5.2), mesh points x_i will be more uniformly distributed in the physical x-space. A Chebyshev polynomial in the transformed ξ- space will be used to approximate the derivative with respect to ξ, and the derivative with respect to x will be computed as follows

$$\frac{d}{dx} = \frac{d}{d\xi}\frac{d\xi}{dx} = \frac{\alpha}{\sin^{-1}\alpha\cos(\sin^{-1}\alpha\xi)}\frac{d}{d\xi}. \tag{5.3}$$

In our computations, we have observed an improvement of one magnitude in the time step with $\alpha = 0.999$; at the same time, the resolution of the numerical method is also enhanced in the interior of the physical domain. We refer the reader to [12] for more details about the evaluation of the transformation.

Uniform Spectral Approximation for Discontinuous functions

We consider the following piecewise C^∞ function

$$g(x) = e^{\sin^2 x} \begin{cases} -\sin(2(x+0.7\pi)) + 1 & -\pi \le x \le -\frac{2}{5}\pi, \\ \sin^2 x & |x| \le \frac{2}{5}\pi, \\ \frac{2}{\pi}x - 1 - \frac{\sin 3x}{6} & \frac{2}{5}\pi < x \le \pi. \end{cases} \tag{5.4}$$

$g(x)$ is defined periodically on the outside of $[-\pi, \pi]$, thus $g(x)$ has three discontinuities in the interval $[0, 2\pi]$. The profile of $g(x)$ is plotted as the solid line in Fig.2. Now, given the mesh value $g(x_i)$, $x_i = \frac{2\pi i}{N}$, $0 \le i \le N$, we use (2.20) and (2.21) to approximate $g(x_{j+\frac{1}{2}})$ and $\frac{d}{dx}g(x_j)$, $0 \le j \le N$ respectively. In Fig. 1(a), (b), we plot the errors in function values and first derivative values respectively in the logarithm scale for different N's, i.e. $N = 32, 64, 128, 256$. In all of the runs, we use a 16th order of exponential cut-off filter and the third order of ENO interpolation in (2.15). We clearly see the uniform convergence and spectral accuracy in the smooth parts of the function $g(x)$.

Linear Advection of Discontinuous Solution with Subcell Resolution

In order to reduce the smearing in contact discontinuities by shock capturing schemes, Harten [10] suggested a sub-cell resolution technique to treat one-dimensional contact discontinuities in the context of the cell-averaged ENO finite difference schemes. Later on, this idea was extended to the point-value version of the ENO finite difference scheme in [17]. We test the subcell resolution by our spectral methods.

Consider the initial boundary value problem of the following linear hyperbolic equation

$$\begin{cases} u_t = u_x, \\ u(x,0) = g(x), & x \in [0, 2\pi] \\ u(0,t) = u(2\pi, t) \end{cases} \tag{5.5}$$

where $g(x)$ is defined in (5.4).

In Fig. 2(a), (b), we plot the numerical solution for $N = 200$ after one and two periodicities, i.e. $t = 2\pi, t = 4\pi$. In both runs, we have used the 10th order exponential cut-off filters.

Inviscid Burgers' Equation

In this classic example of shock wave computation, we consider the initial value problem with sine wave initial conditions,

$$\begin{cases} u_t + (\frac{u^2}{2})_x = 0, \\ u(x,0) = \alpha + \beta \sin x & x \in [0, 2\pi], \\ u(0,t) = u(2\pi, t), \end{cases} \tag{5.6}$$

where $\alpha = 0.3, \beta = 0.7$.

The solution to (5.6) develops a shock discontinuity at time $t = \frac{1}{\beta}$. When $\alpha \neq 0$, the solution consists of a moving shock wave after $t = \frac{1}{\beta}$. As the exact solution for this problem can be obtained by iterative methods, we use this example to test the global accuracy of the scalar **Algorithm I** with $m = 3$ (i.e. the third order of ENO interpolation is used in (3.7)). In table 1, we list the global L_1 error of the numerical solutions and the L_1 error in the smooth regior of the solution at time $t = 2$ and $N = 32, 64, 128, 256$. In computing the global L_1 error, we exclude the occasional one transition point across the shock, and the smooth region is taken as the region which is 0.8 away from the shock location. The third column of Table 1 shows the global third order accuracy in L_1 norm of **Algorithm I**, and the fifth column shows the increasing order of accuracy in the smooth region. In all of the runs, the time step has been chosen such that further decreasing of the time step does not improve the final accuracy. Therefore, the dominant errors come from the spatial discretization. In Fig. 3, solutions at time $t = 2$ and $N = 32$ are plotted (plus) against the exact solution(solid lines). In Fig. 4(a), the errors for $N = 32, 64, 128, 256$ at time $t = 2$ are plotted in logarithm scale. For a comparison, we plot the errors with the same parameters for the third order ENO finite difference scheme in Fig. 4(b).

One-Dimensional Euler Equations for Gas Dynamics

We solve the system of equations (4.1) with different initial data.

1) Interaction of a shock wave and density waves

We consider the following initial condition for (4.1),

$$\begin{cases} \rho_l = 3.857143,\ q_l = 2.629367,\ P_l = 10.333333 & -1 \leq x < -0.8, \\ \rho_r = 1 + \epsilon \sin 5\pi x,\ q_r = 0,\ P_r = 1 & -0.8 < x \leq 1, \end{cases} \tag{5.7}$$

where $\epsilon = 0.2$.

In **Algorithm II**, we choose the third order ENO interpolation and the 16th order exponential cut-off filters. In Fig. 5(a), we display the density profile for $N = 200$ at $t = 0.36$, the solid lines are the solutions obtained by the third order ENO finite difference methods with 800 points. For a comparison, we plot the solution obtained with the second order MUSCL schemes with $N = 200$ in Fig. 5(b).

2) Sod's problem and Lax's problem

We now consider the standard Riemann problem of (4.1) with the following initial data [16],

a) Sod's problem

$$
\begin{aligned}
(\rho_l, q_l, P_l) &= (1, 0, 1) && -1 \le x \le 0, \\
(\rho_r, q_r, P_r) &= (0.125, 0, 0.10) && 0 \le x \le 1;
\end{aligned}
$$

b) Lax's Problem

$$
\begin{aligned}
(\rho_l, q_l, P_l) &= (0.445, 0.698, 3.528) && -1 \le x \le 0, \\
(\rho_r, q_r, P_r) &= (0.5, 0, 0.571) && 0 \le x \le 1.
\end{aligned}
$$

For the Lax's problem, the sub-cell resolution has been applied on the linear degenerated field near contact discontinuities. In both of the problems, we use the third order ENO interpolation in **Algorithm II** and the 10th order exponential cut-off filters. In Fig. 6 (a)-(c) the solutions of the Sod's problems with $N = 150$ at time $t = 0.4$ are plotted, while Fig. 7(a)-(c) display the solutions of the Lax's problem with $N = 150$ at time $t = 0.26$. In both cases, the solid lines are the exact solutions.

Interaction of blast waves

The initial data suggested in [20] to simulate the interactions of two blast waves is as follows

$$
\mathbf{u}(x,0) = \begin{cases} \mathbf{u}_L & 0 \le x \le 0.1, \\ \mathbf{u}_M & 0.1 \le x \le 0.9, \\ \mathbf{u}_R & 0.9 \le x \le 1, \end{cases} \tag{5.8}
$$

where $\rho_L = \rho_M = \rho_R = 1, q_L = q_M = q_R = 0, P_L = 10^3, P_M = 10^{-2}, P_R = 10^2$.

The solutions to this problem possess drastic fluctuations under the impact of interactions; it is a good test of the stability of **Algorithm II**. The complex structure of the solutions after the clash of two blast waves demands a stable high order method to capture the details of solutions. Unlike the finite difference methods, the spectral methods do not require exterior mesh points to treat boundary conditions. We apply characteristic boundary conditions on both boundaries. As the boundaries are treated as solid walls, we impose the condition that velocity variables vanish on both boundaries, i.e. $q_0 = 0, q_N = 0$.

In Fig. 8(a)-(c) and Fig. 9 (a)-(c), we plot the solutions of the state variables with $N = 300$ at time $t = 0.028$ and $t = 0.038$, respectively. The former is an instant before the clash and the latter is one after the clash. The solid lines in both Fig. 8 and Fig. 9 are the solutions obtained with the third order ENO finite difference methods with 800 mesh points. In Fig. 10, the solutions of density with $N = 400$ are also plotted.

Interaction between a Two-dimensional Shock Wave and a Rotating Vortex

The equations in consideration will be (1.1) with

$$\mathbf{u} = (\rho, m_x, m_y, E), \tag{5.9}$$

$$\mathbf{f}(\mathbf{u}) = q_x\mathbf{u} + (0, P, 0, q_x P), \tag{5.10}$$

$$\mathbf{g}(\mathbf{u}) = q_y\mathbf{u} + (0, 0, P, q_y P), \tag{5.11}$$

where q_x, q_y are velocity components in x- and y - directions respectively, $m_x = \rho q_x$ and $m_y = \rho q_y$ are x - and y - momentums respectively . $P = (\gamma - 1)(E - \frac{1}{2}\rho q^2), q^2 = q_x^2 + q_y^2$.

We apply one-dimensional **Algorithm II** on the fluxes $\mathbf{f}(\mathbf{u})$ and $\mathbf{g}(\mathbf{u})$ separately. The right and left eigenvectors for the Jacobian matrices $\frac{\partial \mathbf{f}}{\partial \mathbf{u}}, \frac{\partial \mathbf{g}}{\partial \mathbf{u}}$ can be found in [17].

The physical domain will be the rectangle $[0, 3] \times [-1.5, 1.5]$. A Mach 3 planar shock wave moves from the left to the right. A rotating vortex is initially located to the right side of the shock. As the time progresses, the shock will hit the vortex and interact with it. The shock front will be deformed by the interaction, and pressure waves are generated from the interactions. In the computations, we define the velocity fields of the vortex as those induced by two rotating concentric cylinders with radius r_1 and r_2 respectively, $r_1 < r_2$. Initially the vortex is located at (x_c, y_c). The outside cylinder is stationary and the inside one rotates with the angular velocity ω. Let $\tilde{v}(r)$ be the radius velocity at a distance r from the center of the vortex, we have

$$\tilde{v}(r) = \begin{cases} \omega r & \text{if } 0 \le r \le r_1, \\ \omega \frac{1}{r}(\frac{1}{ra} + \frac{rr_1^2}{b}) & \text{if } r_1 \le r \le r_2, \\ 0 & \text{if } r \ge r_2, \end{cases} \tag{5.12}$$

where $a = \frac{1}{r_1^2} - \frac{1}{r_2^2}, b = r_1^2 - r_2^2, r = \sqrt{(x - x_c)^2 + (y - y_c)^2}$. We choose $r_1 = 0.15, r_2 = 0.75, \omega = 7.5$.

Therefore the x - and y - velocities induced by this vortex at (x, y) will be

$$\tilde{q}_x = -\frac{y - y_c}{r}\tilde{v}(r), \tag{5.13}$$

$$\tilde{q}_y = \frac{x - x_c}{r}\tilde{v}(r), \tag{5.14}$$

where $x_c = 2.25, y_c = 0$.

The initial conditions for the simulation will be as follows:

$$\rho_l = 3.857143,$$

$$q_{xl} = 2.629367 \qquad \text{if } x < x_0,$$

$$q_{yl} = 0, \tag{5.15}$$

$$P_l = 10.333333, \tag{5.16}$$

and

$$\begin{aligned} \rho_r &= 1, \\ q_{xr} &= \tilde{q}_x \qquad \text{if } x > x_0, \\ q_{yr} &= \tilde{q}_y, \\ P_r &= 1, \end{aligned} \tag{5.17}$$

where x_0 is the initial shock position, $x_0 = 1.5$.

We impose characteristic boundary conditions on both left and right boundaries. A periodic boundary condition is considered in the y-direction and hence we are actually simulating the interaction between an array of periodically distributed vortices and a planner shock wave. To relax the time restrictions of the Chebyshev approximation in the x - direction, we apply the mesh transformation (5.2) with $\alpha = 0.999$. The shock has been made stationary by a translation in the mean flow direction. The second order ENO interpolation and the 10-th order exponential filter have been used in (4.10).

Fig. 11(a),(b) are the contour plots of the pressure and density fields at time $t = 0.4$, while Fig. 12(a),(b) are the close-ups of the pressure and density at time $t = 0.4$. Fig. 13 is the pressure profile at time $t = 0.4$.

Concluding Remarks

Centered difference methods including spectral methods are efficient and accurate, while upwinding difference methods offer the advantages of sharp monotonic shock profiles. We have explored, in this work, the possibilities of blending the advantages of the ENO finite difference methods and the spectral methods. Numerical results have shown the robustness and feasibility of this approach at a small extra cost over the standard spectral methods.

ACKNOWLEDGMENT

We would like to thank Professor David Gottlieb for many useful discussions and Dr. Waison Don for suggestions on several computational issues.

References

[1] J. P. Boris, and D. L. Book, "Flux-Corrected Transport I: SHASTA - A Fluid Transport Algorithm that Works",J. Comput. Phys., 11 (1973), pp. 38-69.

[2] Wei Cai, "Essentially Non-Oscillatory Spectral Methods for Shock Wave Computations", Ph.D. Thesis (1989), Brown University, Division of Applied Mathematics, Providence, R.I.

[3] W. Cai, D. Gottlieb and A. Harten, "Cell Averaging Chebyshev Methods for Hyperbolic Problems", to appear in Computers and Mathematics with Applications, Advances in PDE (1990 annual issue).

[4] W. Cai, D. Gottlieb, and C.-W. Shu, "Essentially Non-Oscillatory Spectral Fourier Method for Shock Wave Calculations" Math. Comput., Vol. 52, No. 186, April 1989, pp. 389-410.

[5] C. Canuto, M.Y. Hussaini, A. Quarternoni, and T. A. Zang *Spectral Methods in Fluid Dynamics* Springer-Verlag (1988).

[6] B. Engquist, P. Lotstedt, and B. Sjogreen, "Non-linear Filters for Efficient Shock Computations", Math. Comput., Vol. 52, April 1989, pp. 509-537.

[7] D. Gottlieb, and S. Orzarg *Numerical Analysis of Spectral Methods: Theory and Applications* (SIAM-CBMS, Philadephia, 1977).

[8] D. Gottlieb, and E. Tadmor "Recovering Pointwise Values of Discontinuous Data Within Spectral Accuracy," in *Progress and Supercomputing in Computational Fluid Dynamics*, ed. by E.M. Murman, S.S. Abarbanel (Birkhaeser, Boston) pp. 357-375 (1985).

[9] A. Harten, B. Engquist, S. Osher, and S. Chakravarthy, "Uniformly high order accurate non-oscillatory schemes, III," J. Comput. Phys., 71 (1987), pp. 231-303.

[10] A. Harten, "ENO Schemes with Subcell Resolutions" J. Comput. Phys., 83 (1989), pp. 148-184.

[11] A. Harten, and J. M. Hyman,"A self Adjusting Grid for the Computation of Weak Solutions of Hyperbolic Conservation Laws", *J. Comp. Phys.*, V. 50(1983), pp. 235-269.

[12] D. Kosloff, and Tal-Ezer Hillel, "Modified Chebyshev Pseudo-spectral Method with $O(\frac{1}{N})$ Time Step Restriction", Icase Report 89-71, (December, 1989).

[13] F. Lafon, and S. Osher, "High Order Filtering Methods for Approximating Hyperbolic Systems of Conservation Laws", Icase Report 90-25 (March, 1990).

[14] A. Madja, J. McDonough, and S. Osher "The Fourier Method for Nonsmooth Initial Data," Math. Compt. 32, 1041-1081 (1978).

[15] P. Roe, "Approximate Riemann Solvers, Parameter Vectors, and Difference Schemes, " J. Compt. Phys., V. 43 (1981), pp. 357-372.

[16] G. A. Sod, " A Survey of Several Finite Difference Methods for Systems of Nonlinear Hyperbolic Laws," J. Compt. Phys., V. 27 (1978), pp. 1-31.

[17] C.-W. Shu and S. Osher, "Efficient Implementation of Essentially Nonoscillatory Shock-Capturing Schemes, II," J. Compt. Phys., V. 83, No. 1, July 1989.

[18] H. Vandeven "Family of Spectral Filters For Discontinuous Problems," Preprint of Centre De Mathematiques Appliquees (Unite de Recherche Associee au CNRS - 756), Ecole Polytechnique , France (April, 1987).

[19] B. van Leer, "Toward the Ultimate Conservative Difference Schemes V. A Second Order Sequel to Godunov Method, " J. Compt. Phys., V. 32 (1979), pp. 101-136.

[20] P. Woodward, and P. Colella, "The Numerical Simulation of Two-Dimensional fluid Flows with Strong Shock," J. Compt. Phys., V. 54(1984), pp. 115-173.

Table 1: Global L_1 error and L_1 error in the smooth region for the Burgers' equations at time $t = 2$, the smooth region is defined to be 0.8 away from the shock location

N	Global	Order	Smooth region	Order
32				
	1.49(-4)		1.17(-4)	
64		2.5		4.3
	2.70(-5)		5.86(-6)	
128		2.9		6.5
	3.70(-6)		6.54(-8)	
256		3.7		10.0
	2.95(-7)		6.36(-11)	

Figure 1. Walsh Spectral Approximations to Discontinuous Functions, N=32,64,128,256.
(a) Errors in Function Values in Logarithm Scale;(b) Errors in First Derivatives.

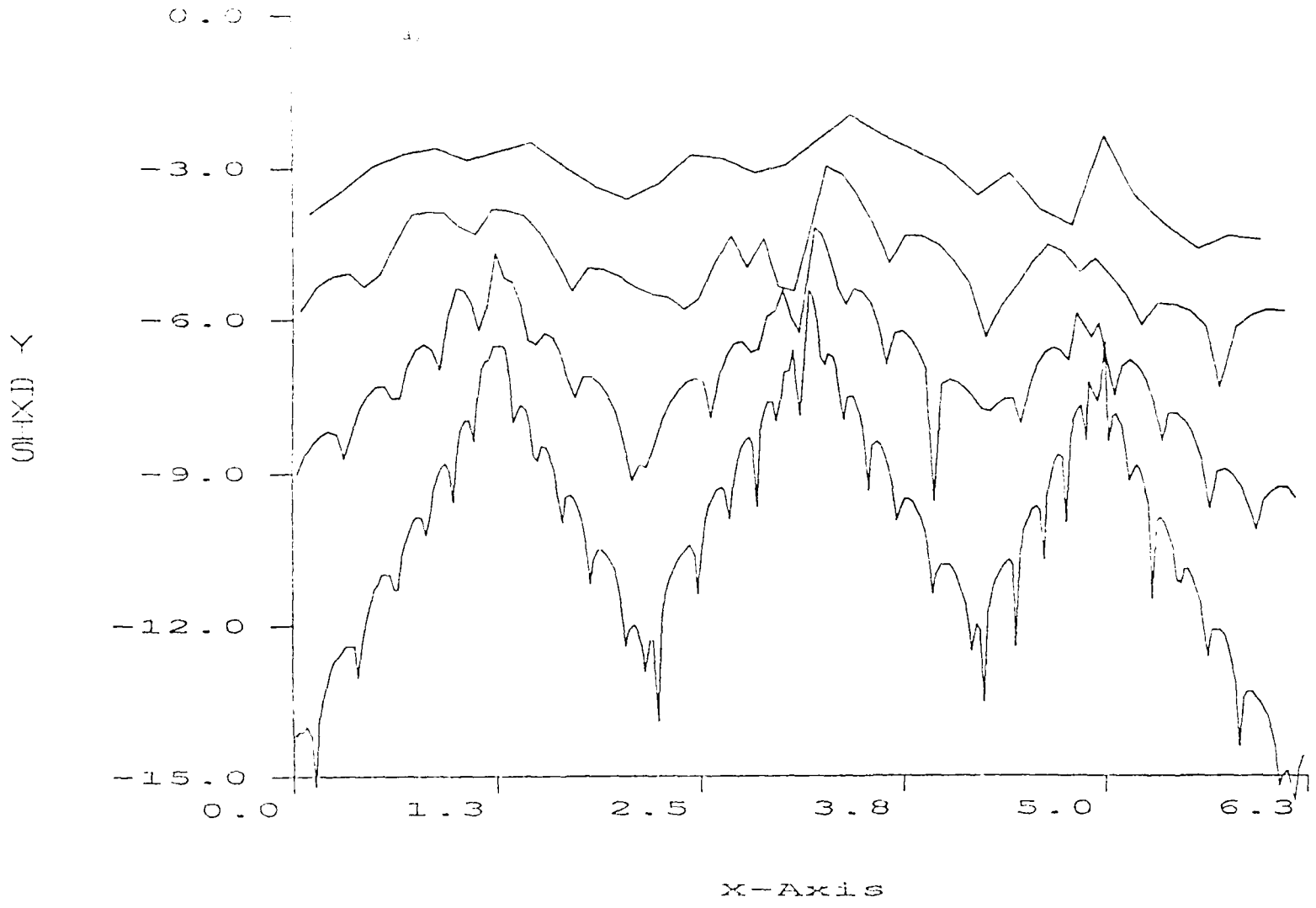

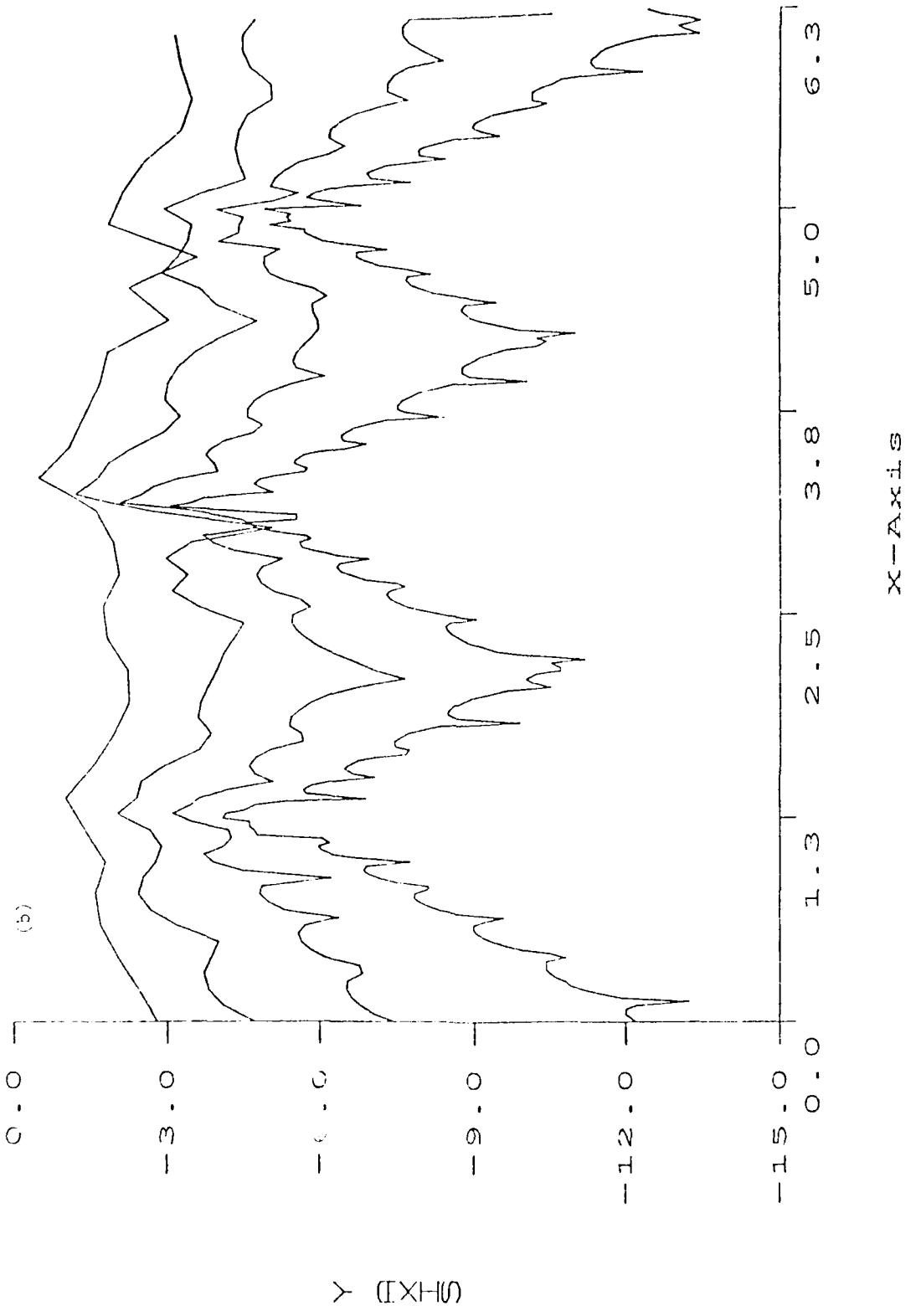

Figure 1. (continued)

Figure 2. Linear Advection of Discontinuous Solutions with Subcell Resolutions, N=200
(a) time t = 2π; (b) time t = 4π

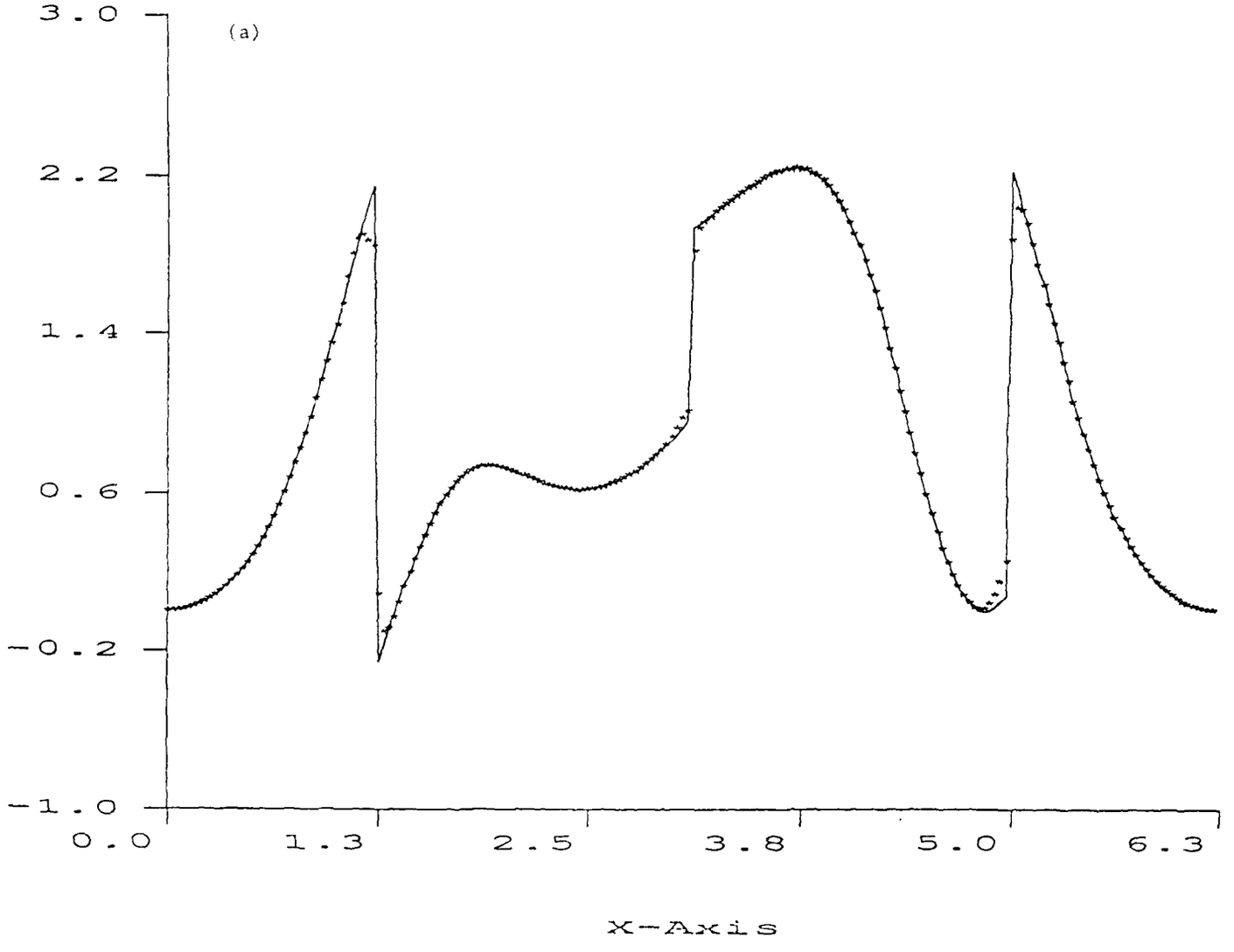

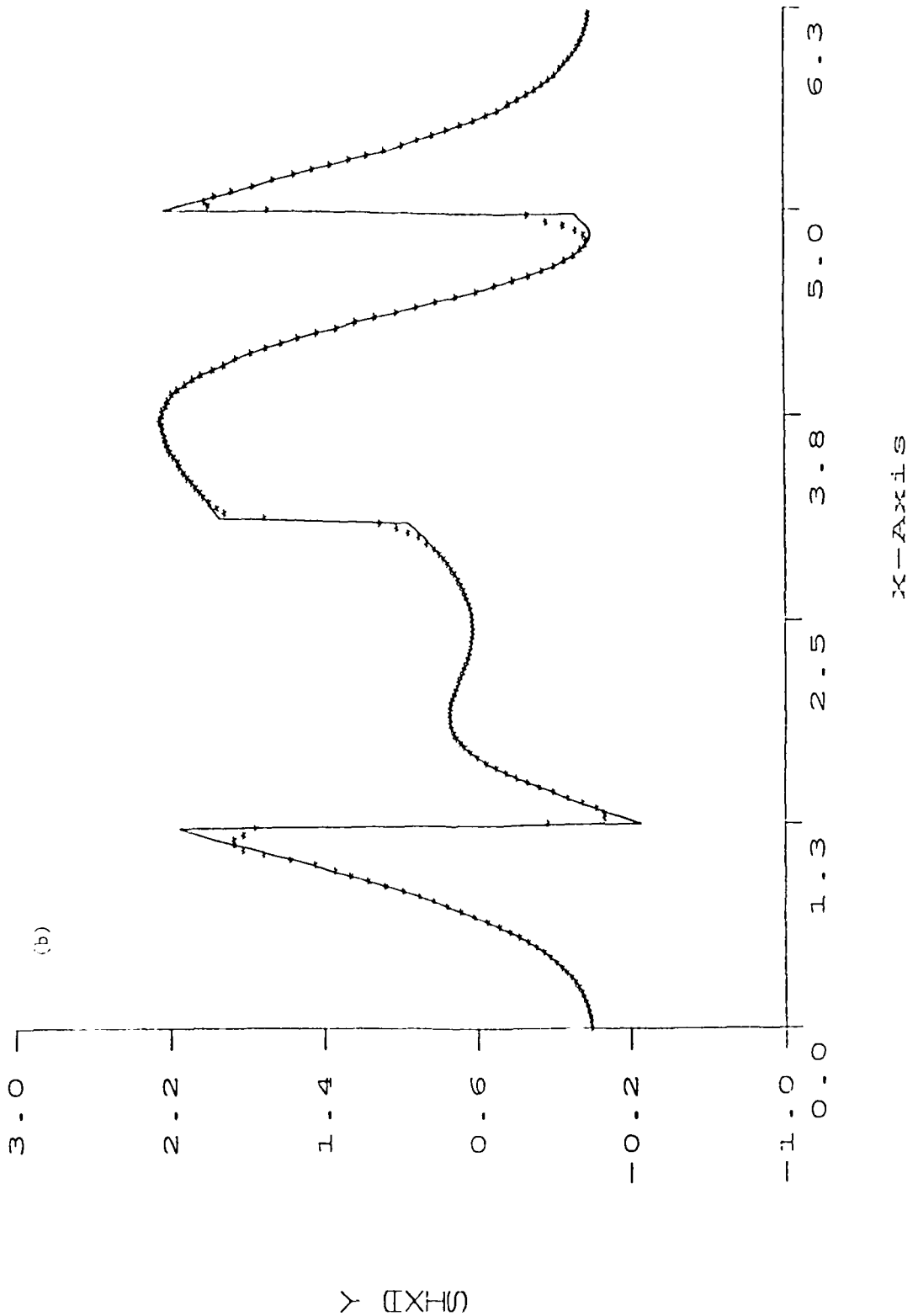

(b)

Figure 2. (Continued)

Figure 3. Solutions to the Inviscid Burgers' Equation with Algorithm I, N = 32, t = 2. Numerical Solutions (plus), Exact Solutions (solid lines).

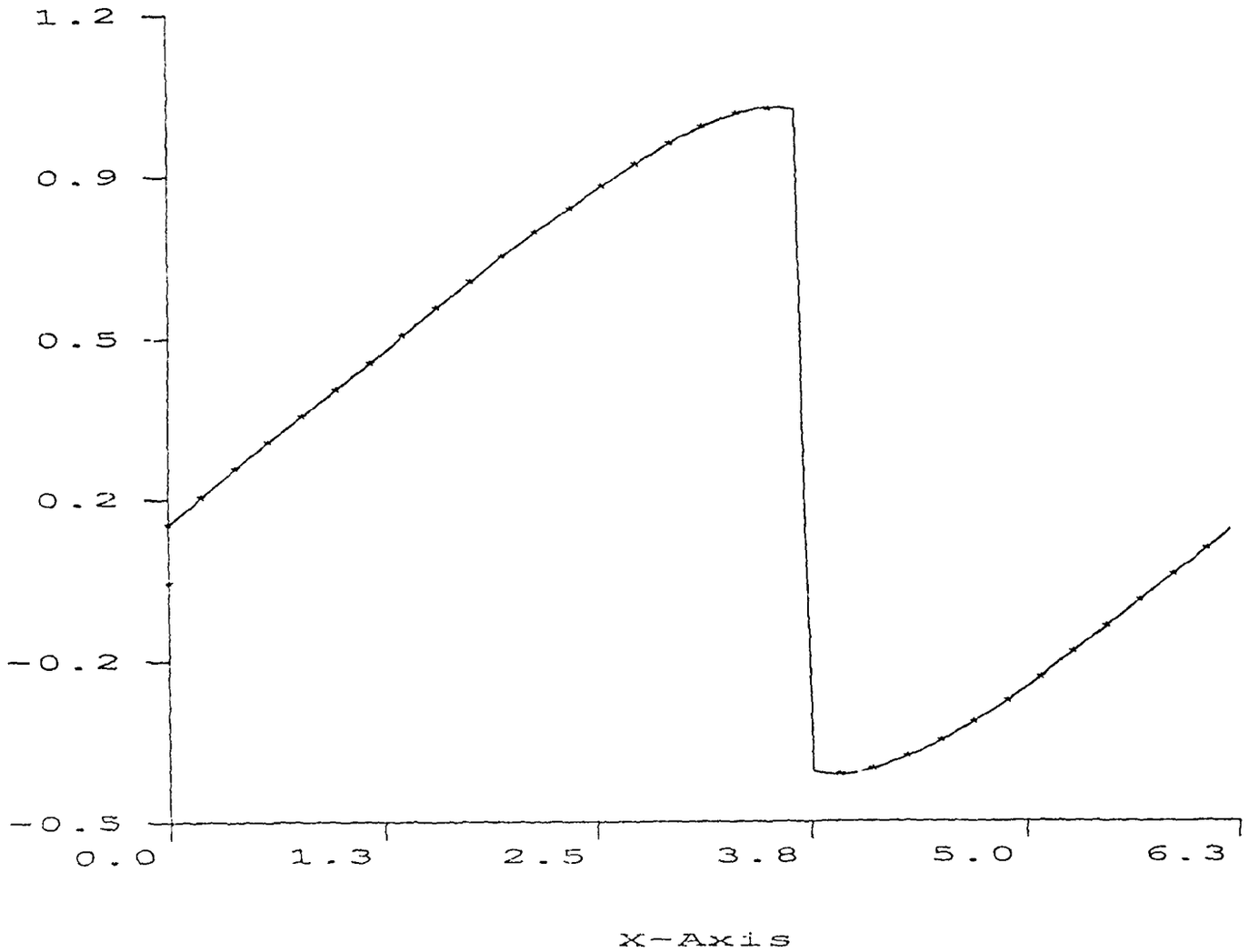

Figure 4. Errors to the Inviscid Burgers' Equation for N = 32, 64, 128, 256, at time t = 2.
(a) the Spectral Algorithm I, (b) the Third Order ENO Finite Difference Methods.

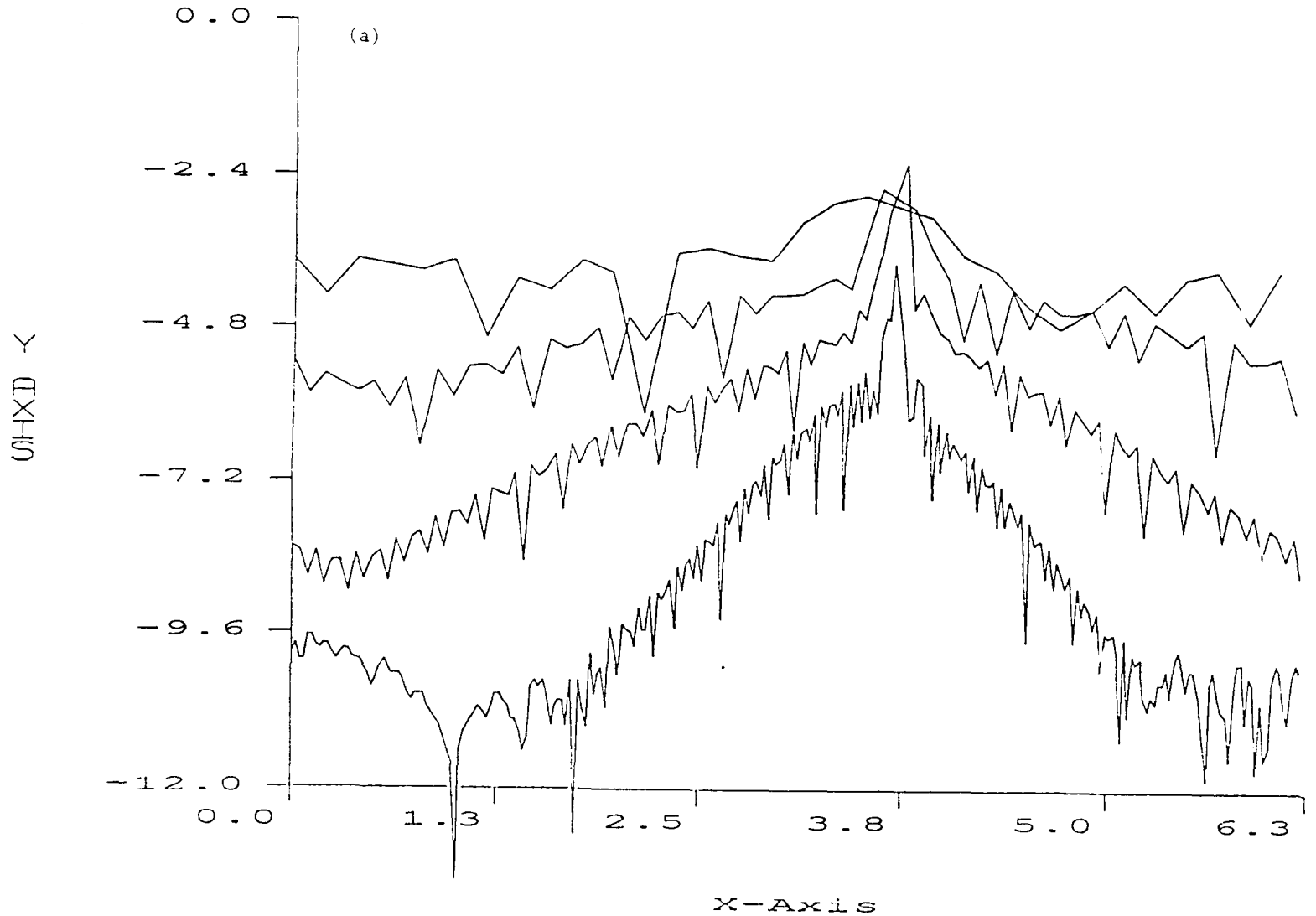

Figure 4. (Continued)

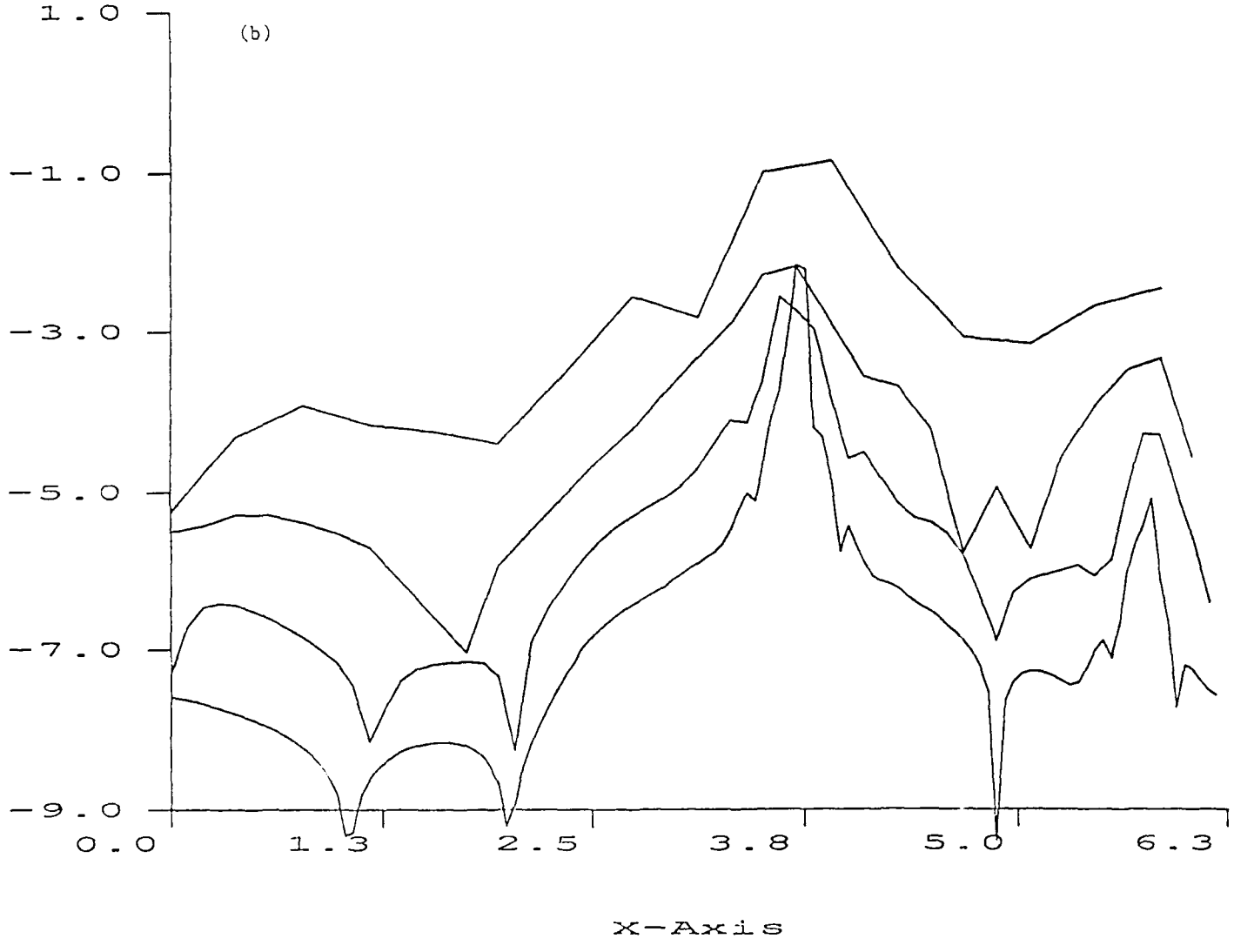

Figure 5. Interactions between One-Dimensional Shock Wave and Density Waves with N = 200 at Time t = 0.36. Density (a) the Spectral Algorithm I, (b) the Second order MUSCL Scheme.

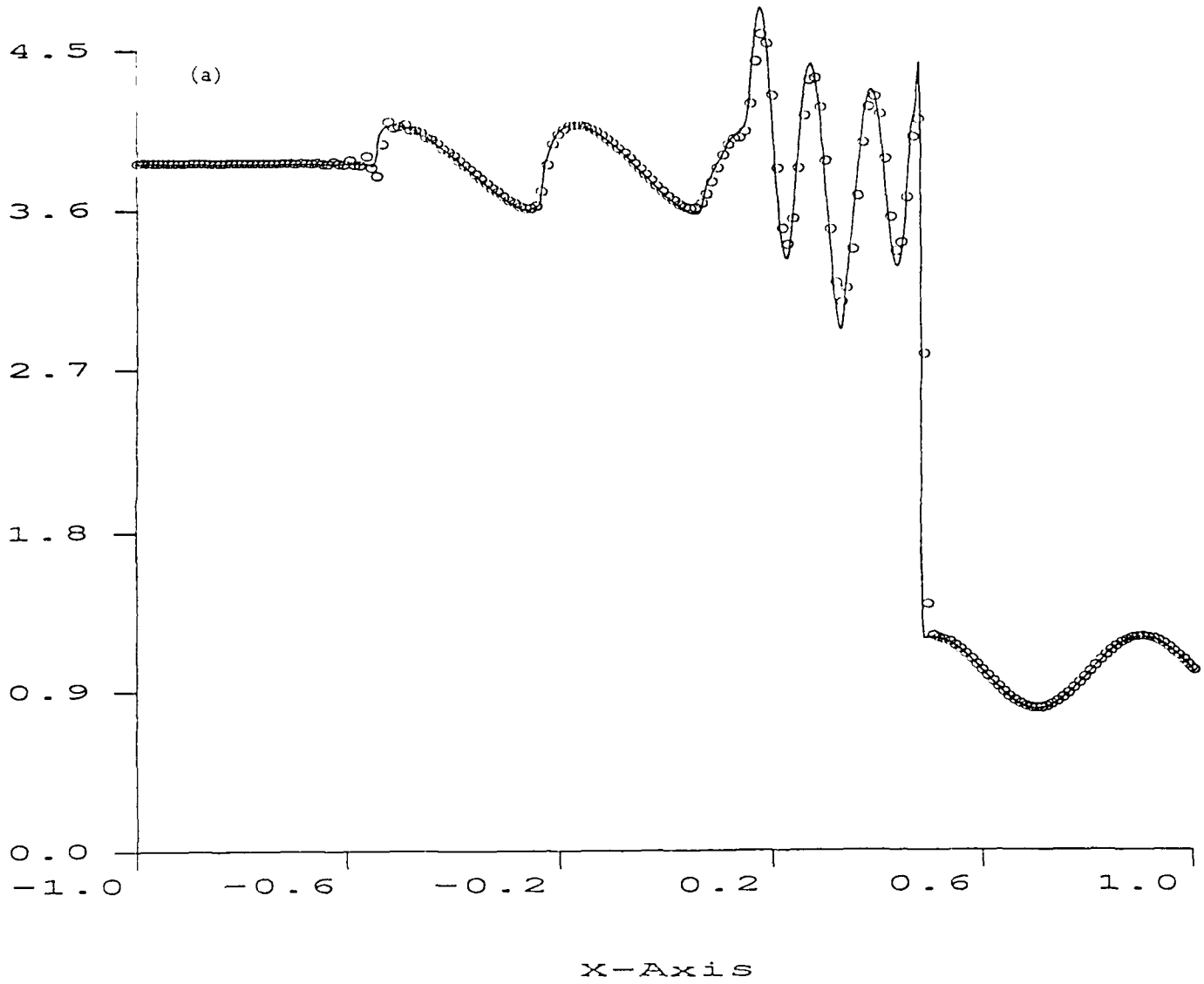

Figure 5. (Continued)

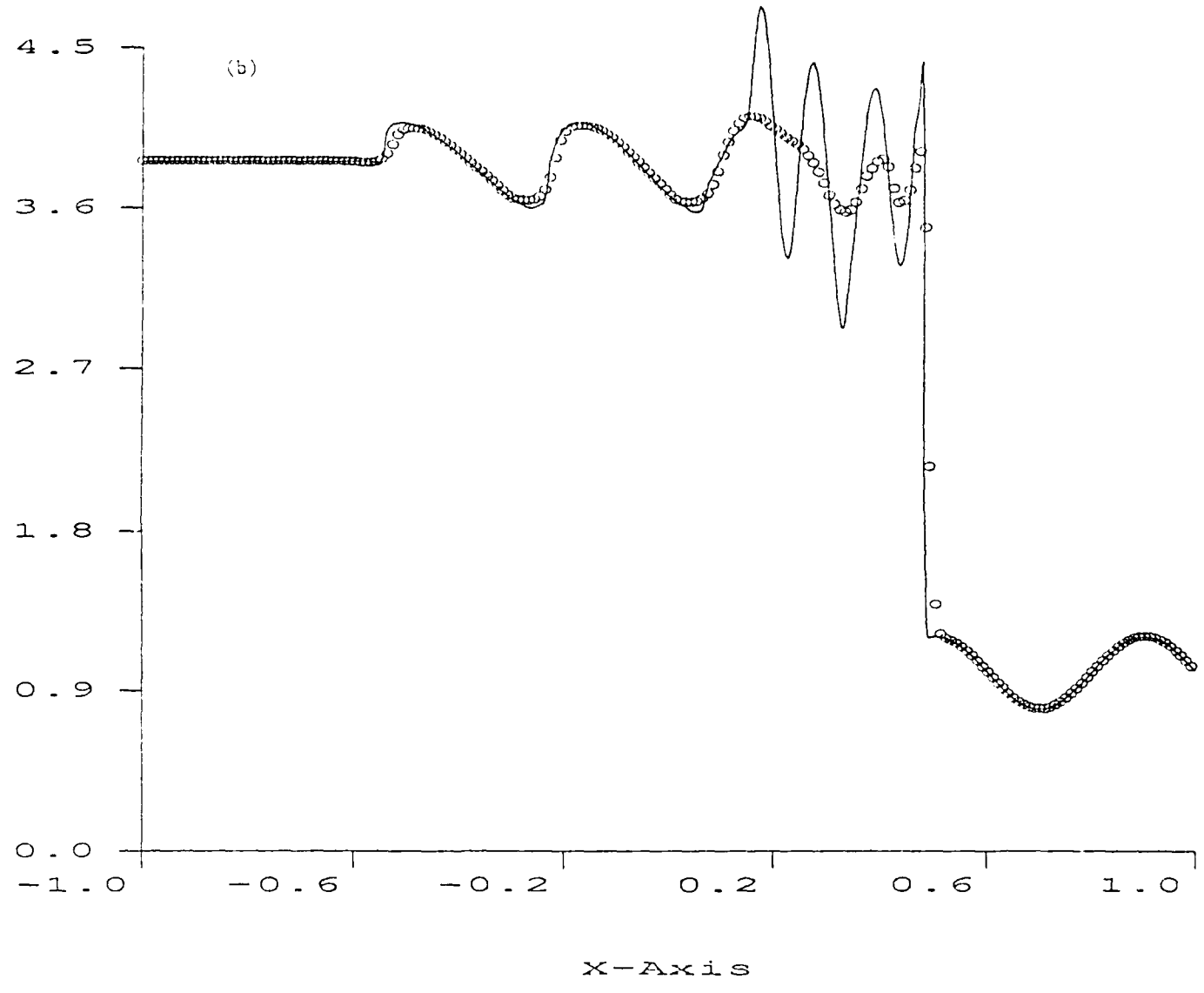

Figure 6. Solutions of the Sod's Problem with N = 150 at Time t = 0.4. (a) Density, (b) Velocity, (c) Pressure.

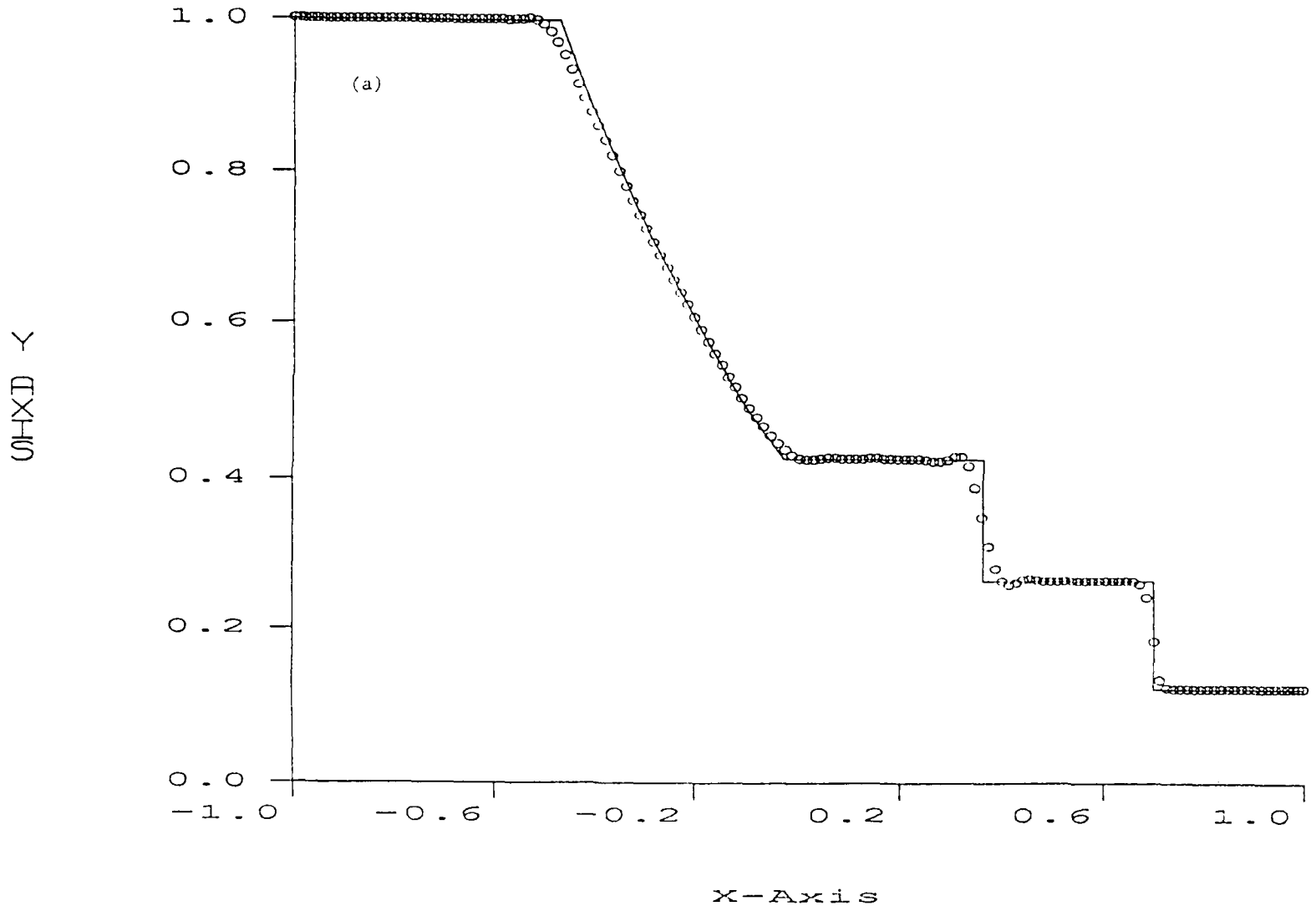

Figure 6. (Continued)

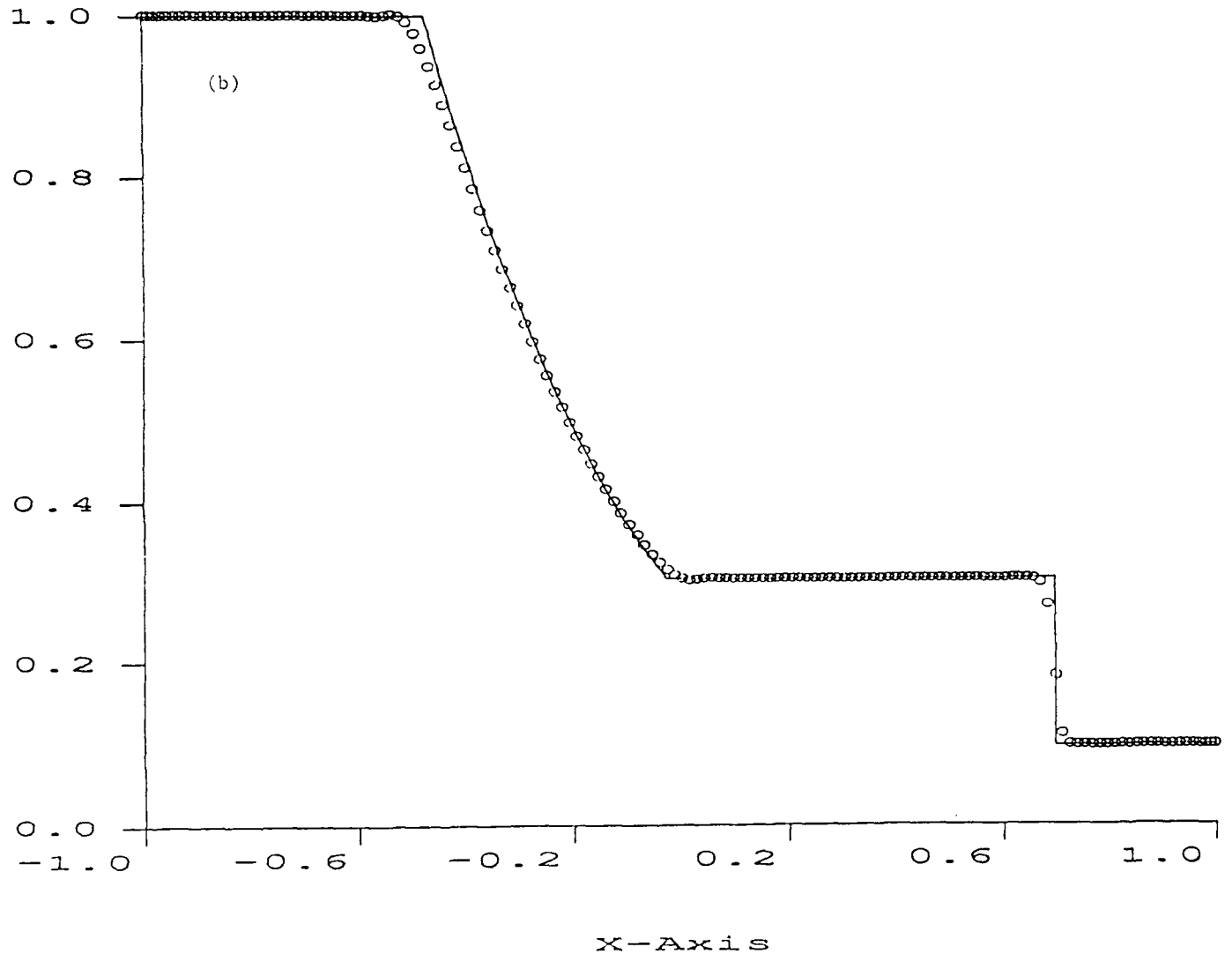

Figure 6. (Continued)

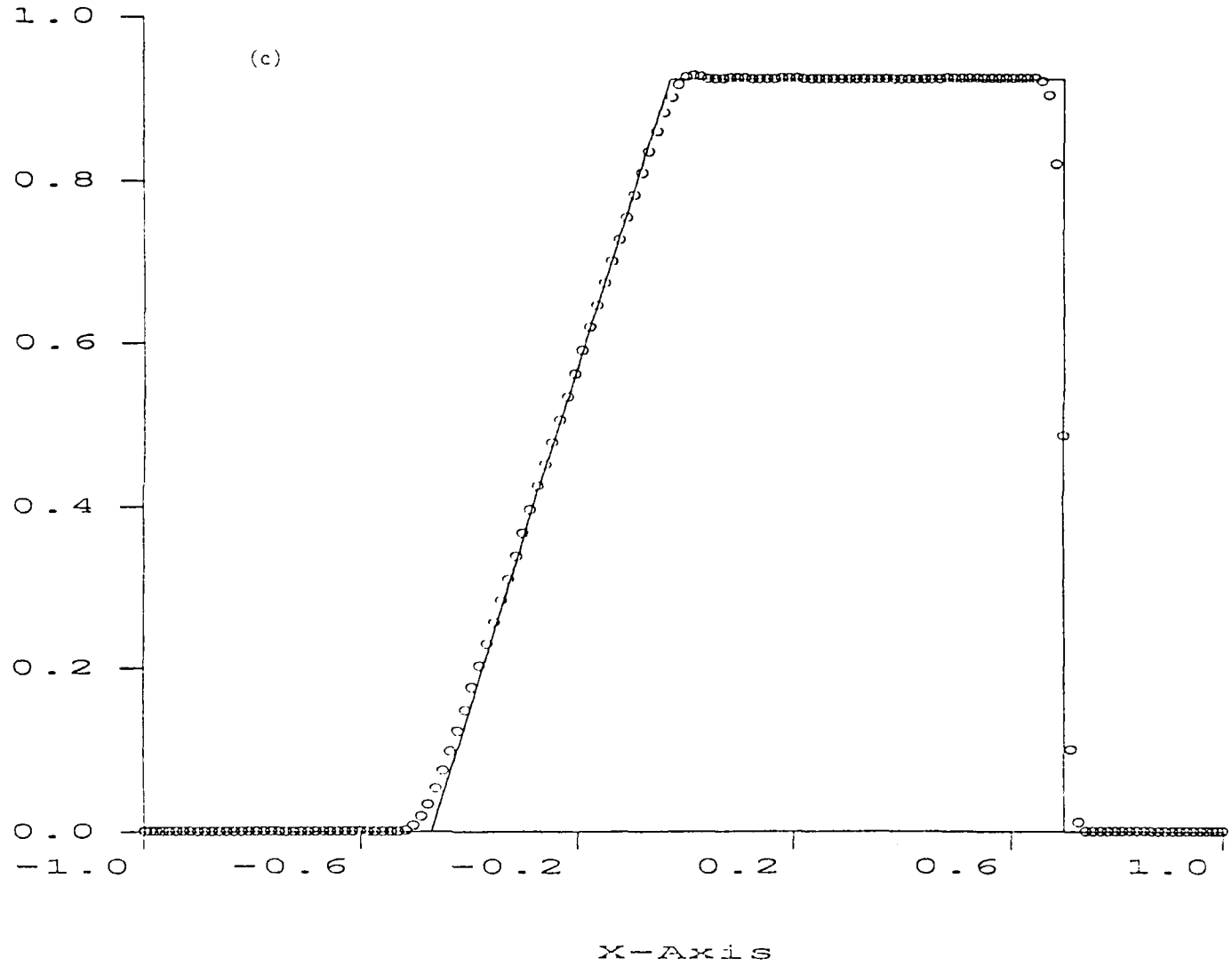

Figure 7. Solutions of the Lax's Problem with N = 150 at time t = 0.26. (a) density, (b) velocity (c) Pressure.

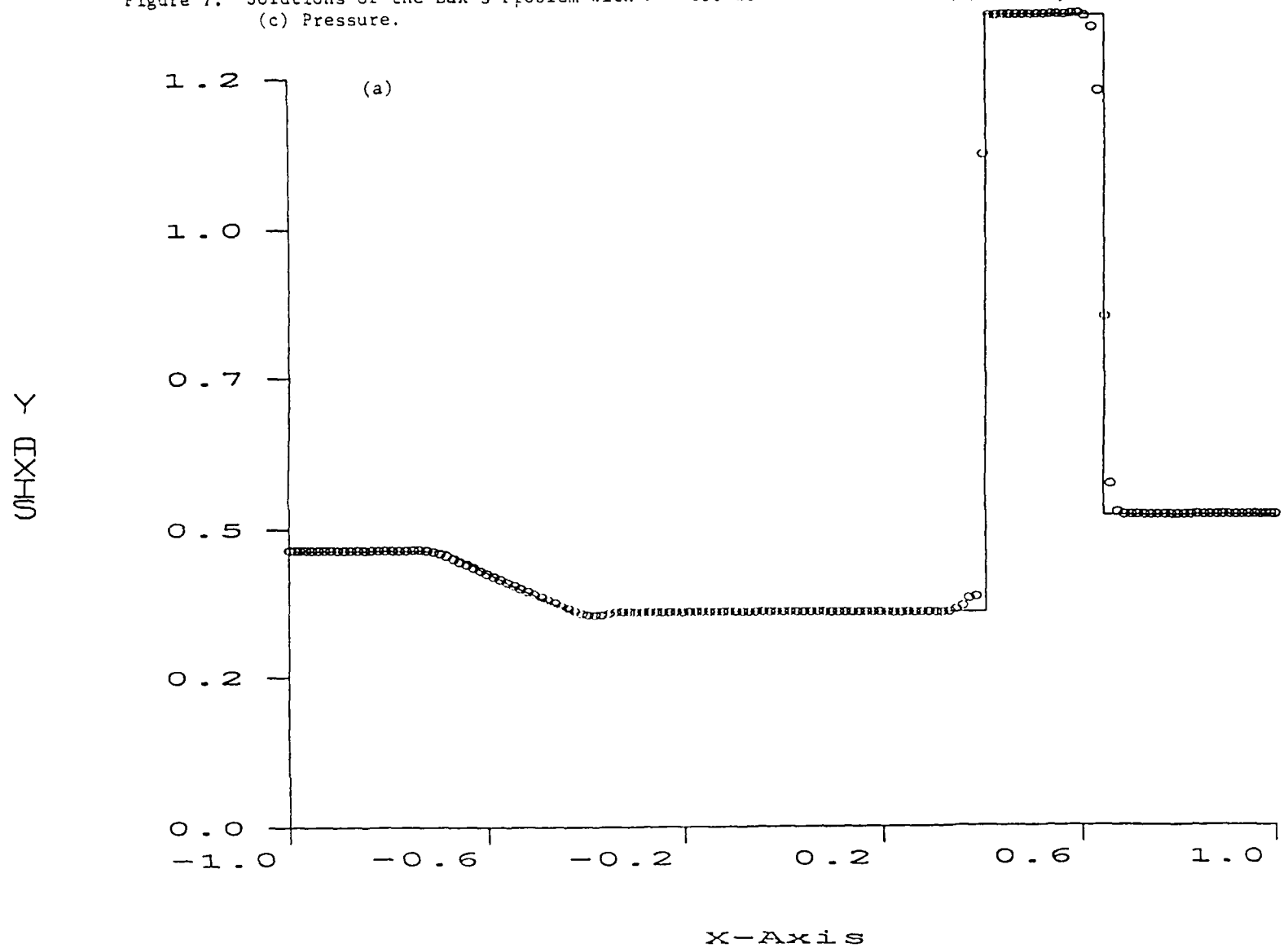

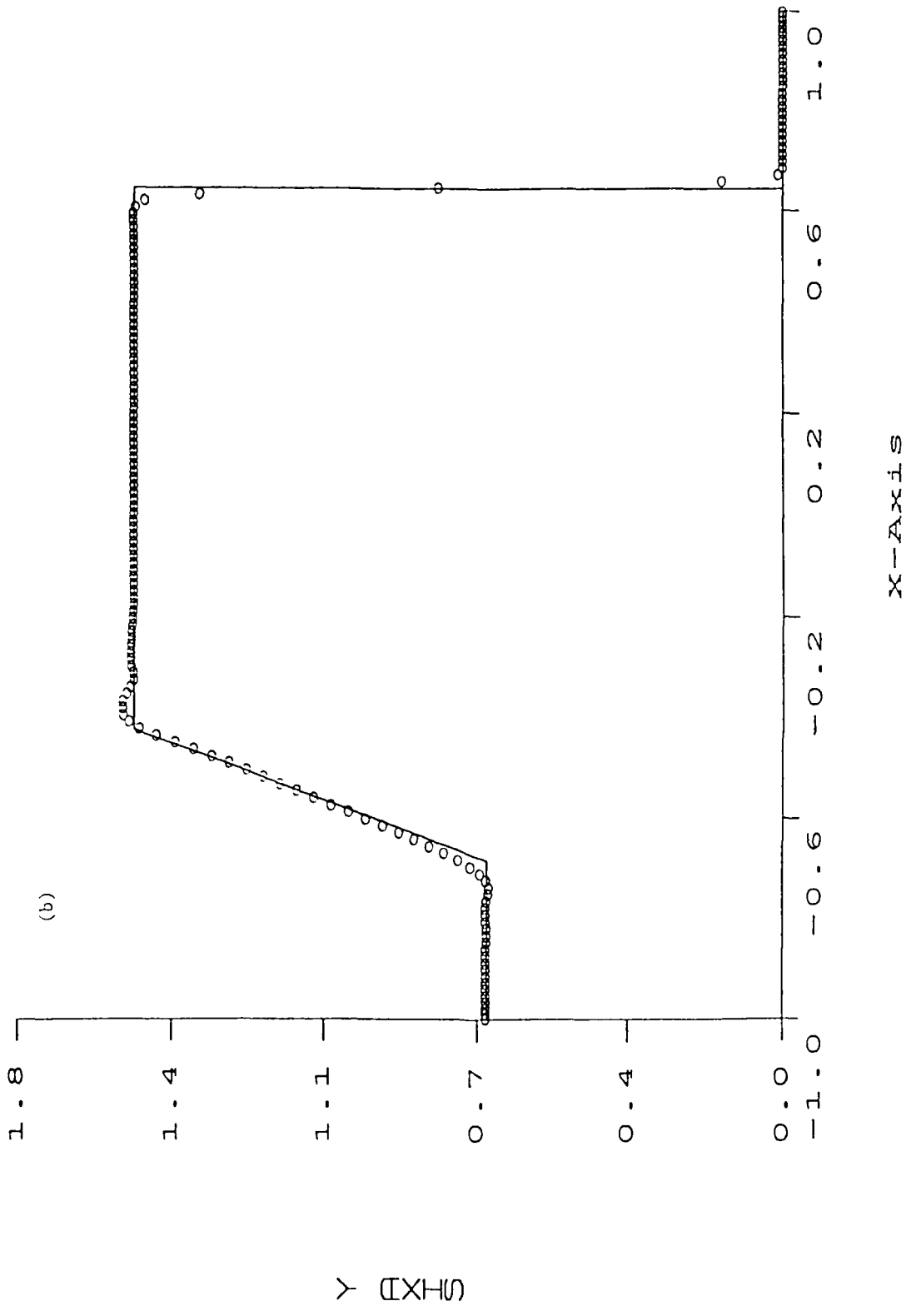

Figure 7. (Continued)

Figure 7. (Continued)

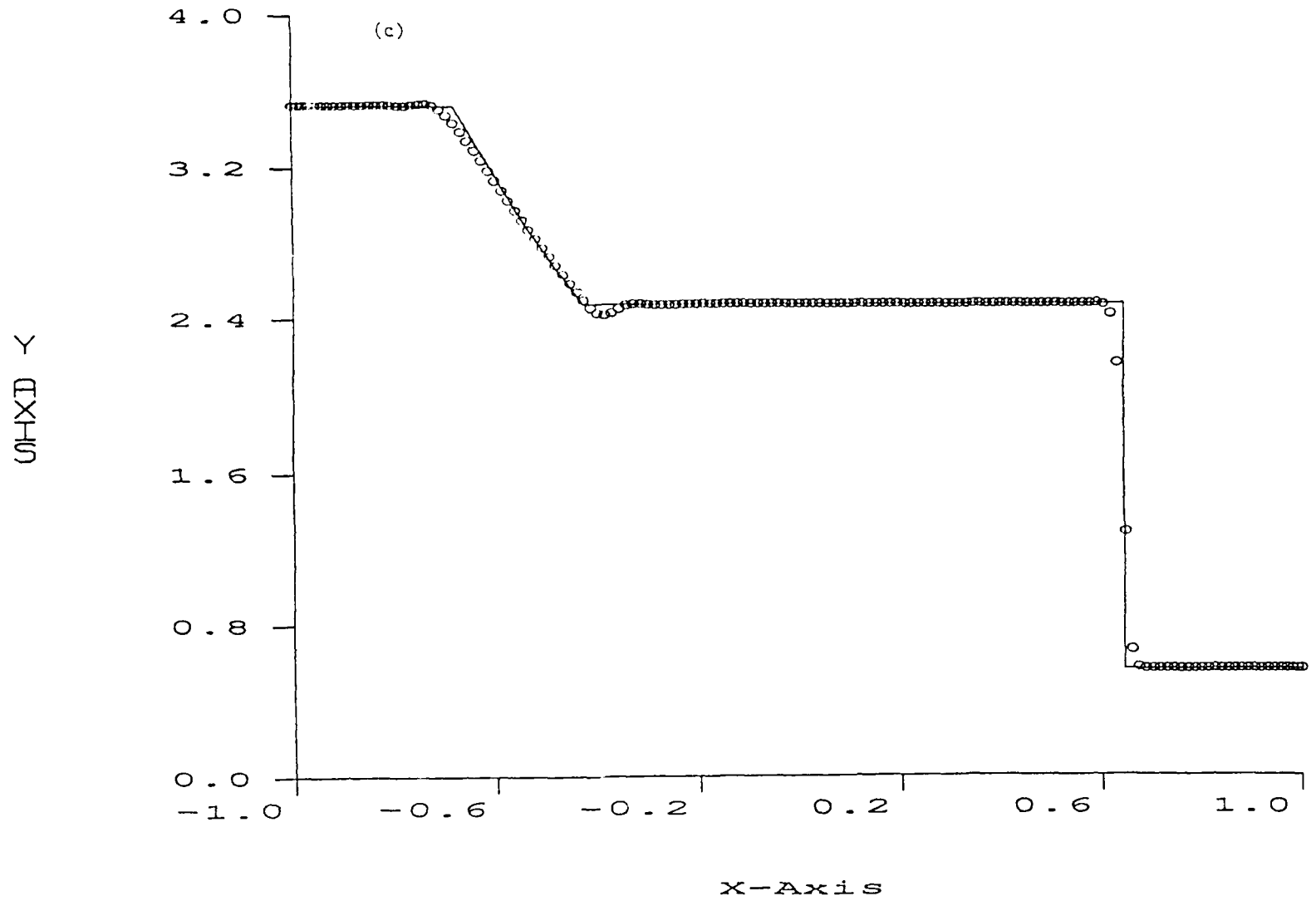

Figure 8. Blast Wave Problem with N = 300 at Time t = 0.028. (a) Density, (b) Velocity,(c) Pressure.

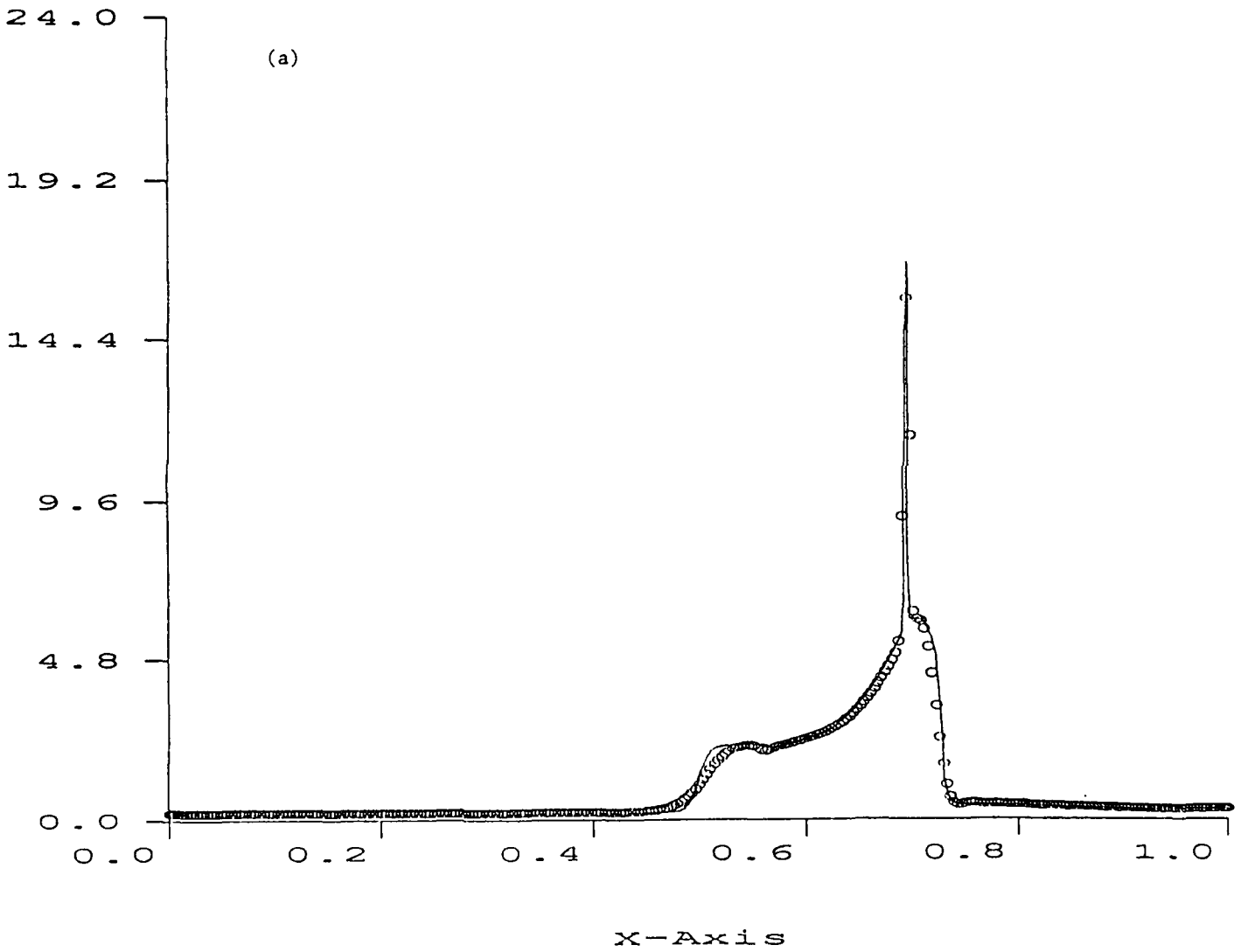

Figure 8. (Continued)

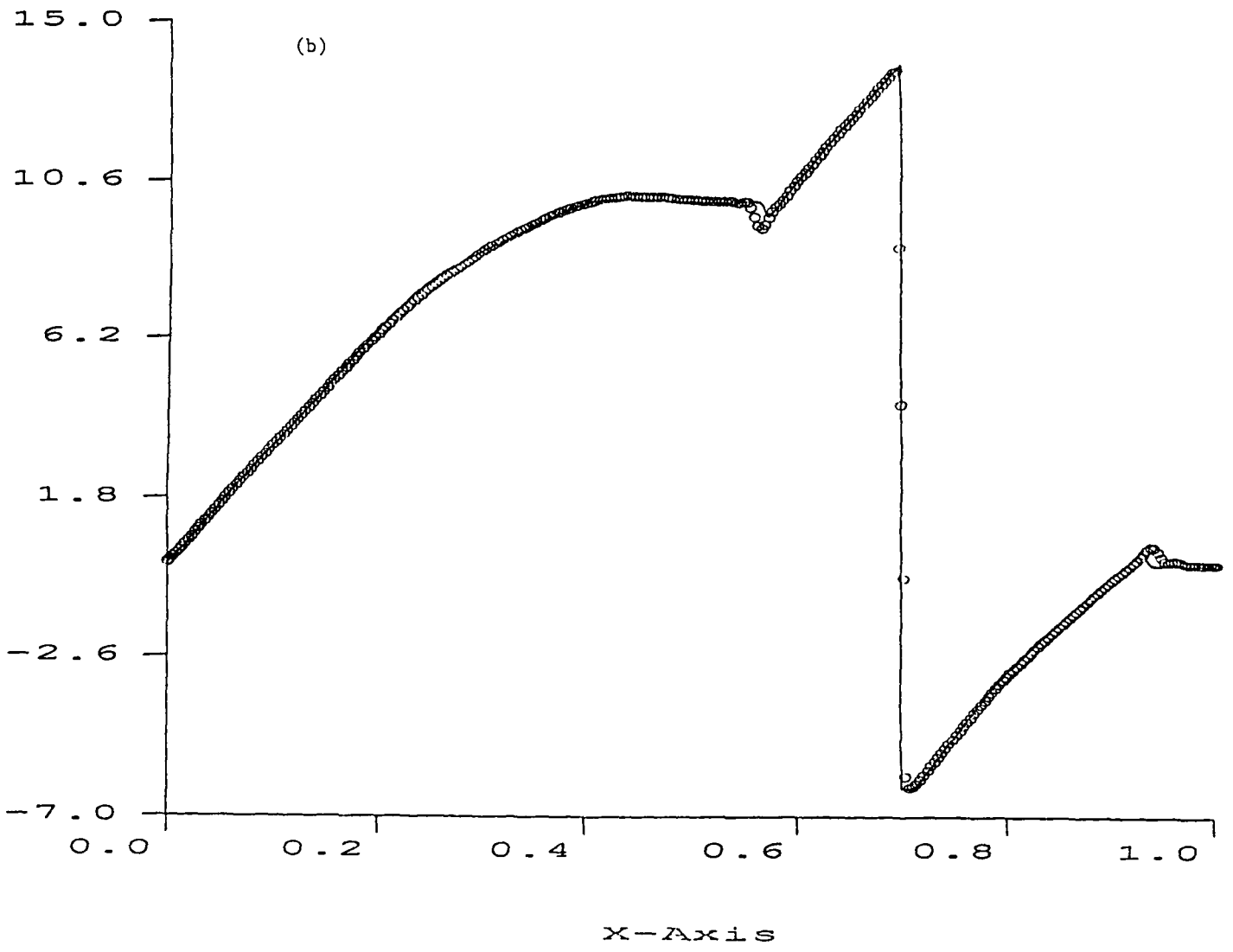

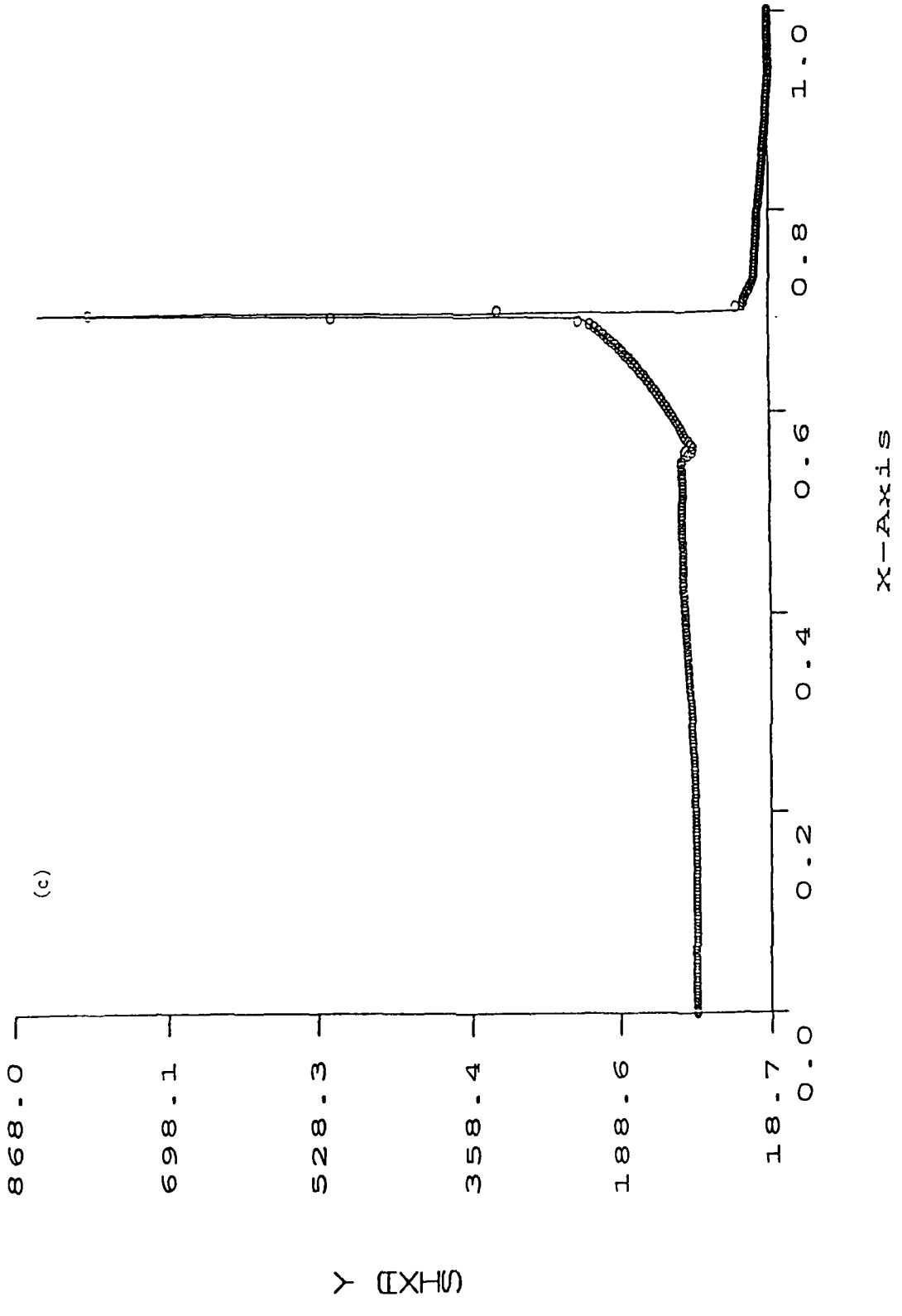

Figure 8. (Continued)

Figure 9. Blast Wave Problem with N = 300 at Time t = 0.038. (a) Density, (b)Velocity, (c) Pressure.

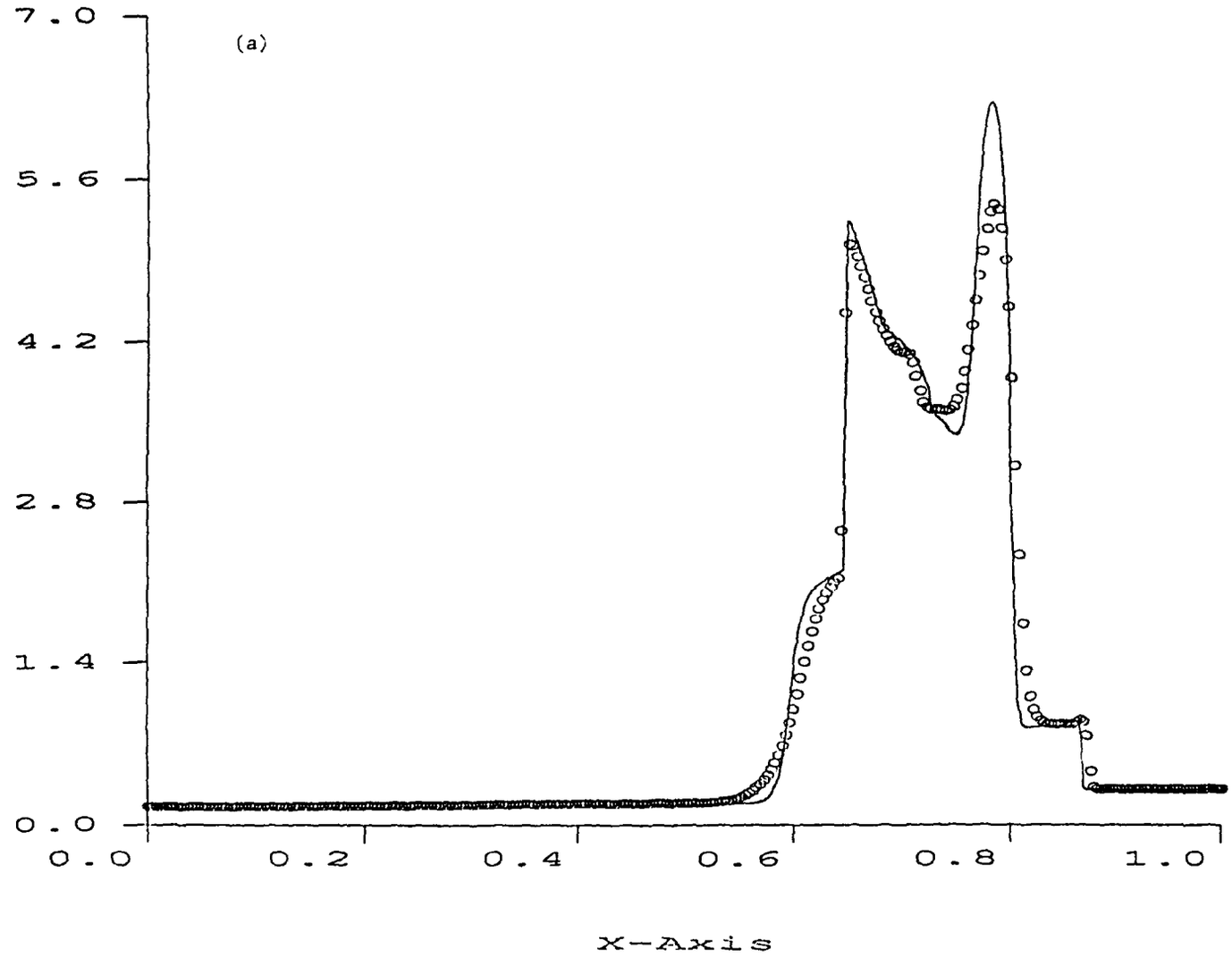

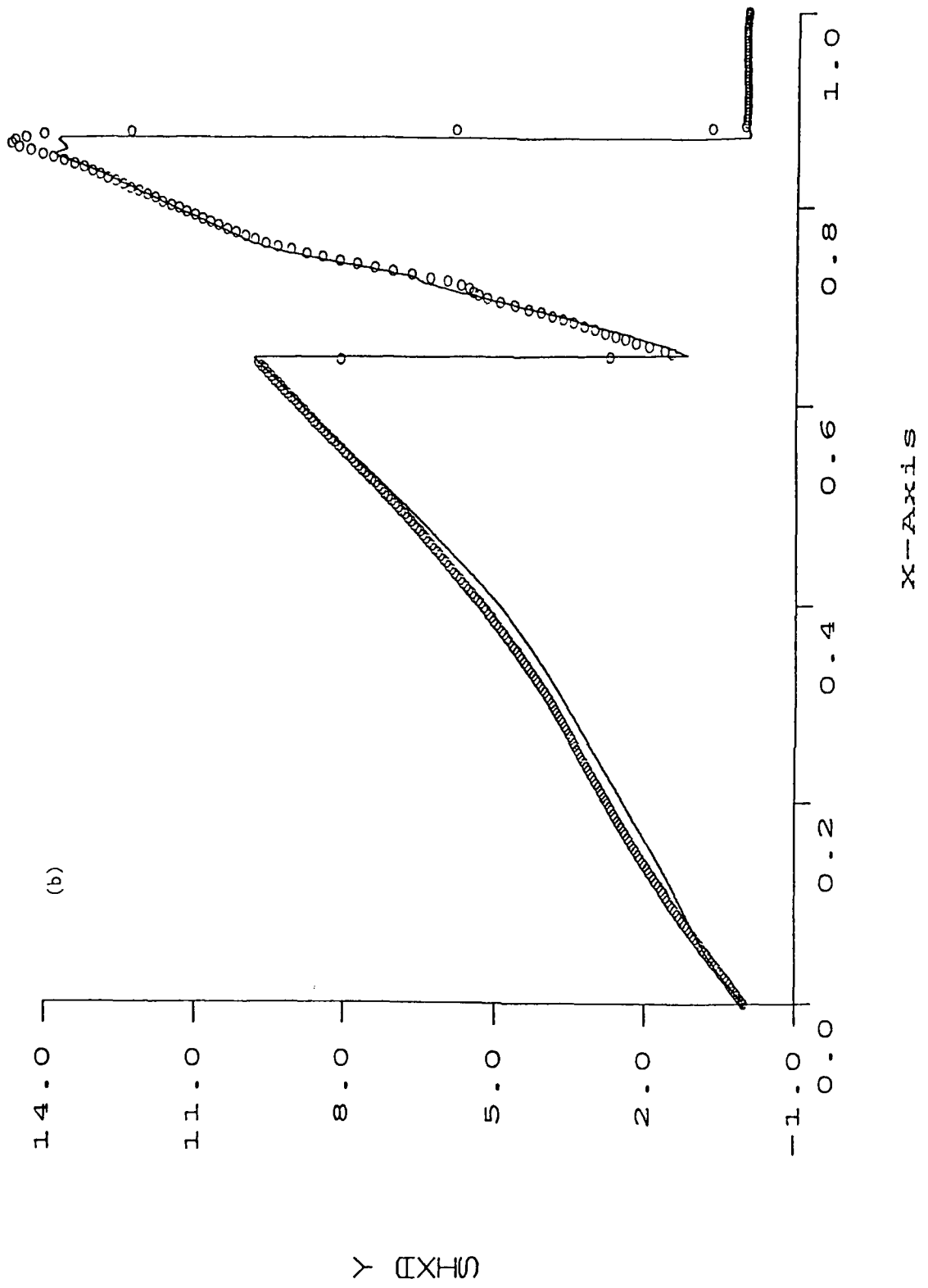

Figure 9. (Continued)

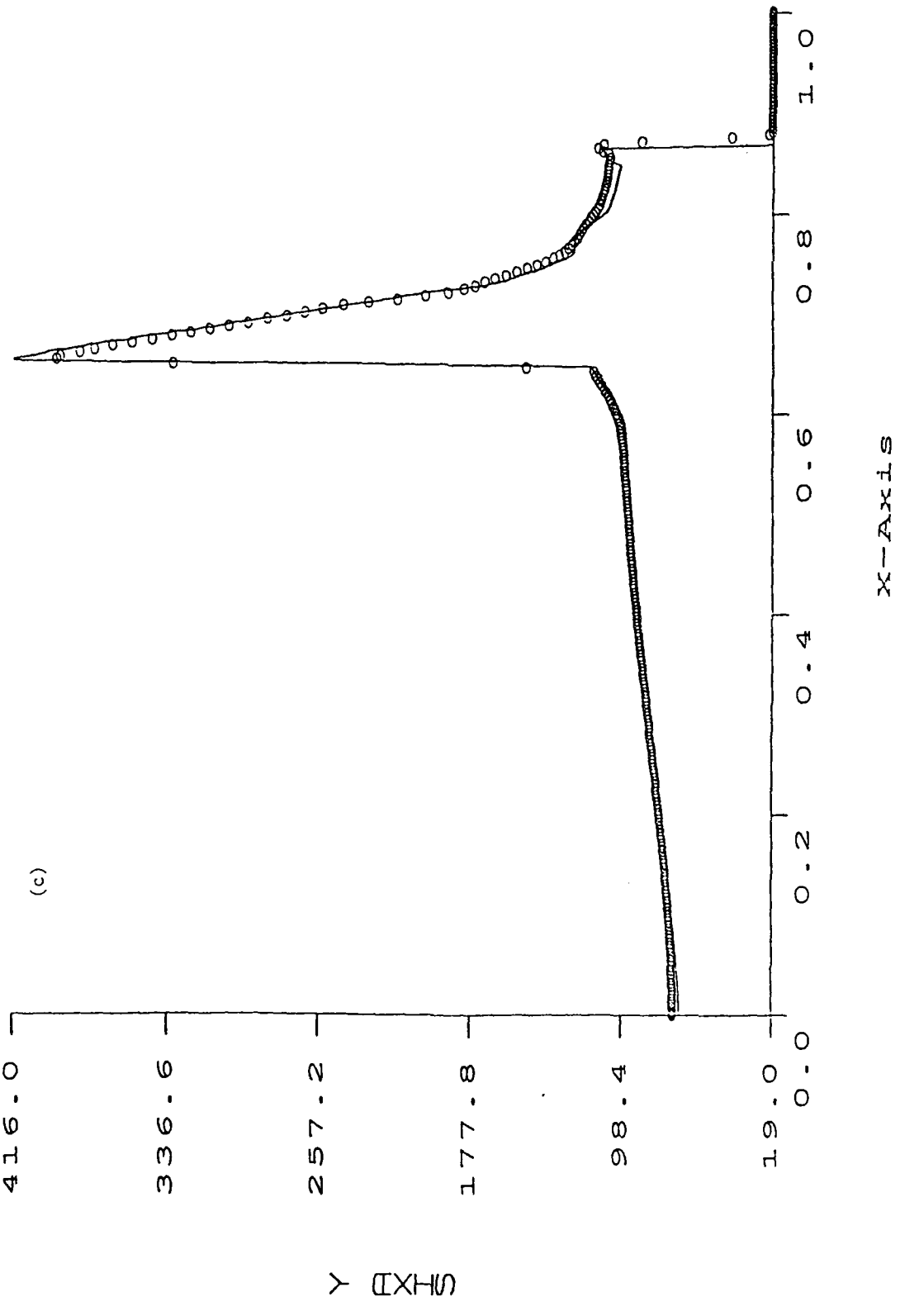

Figure 9. (Continued)

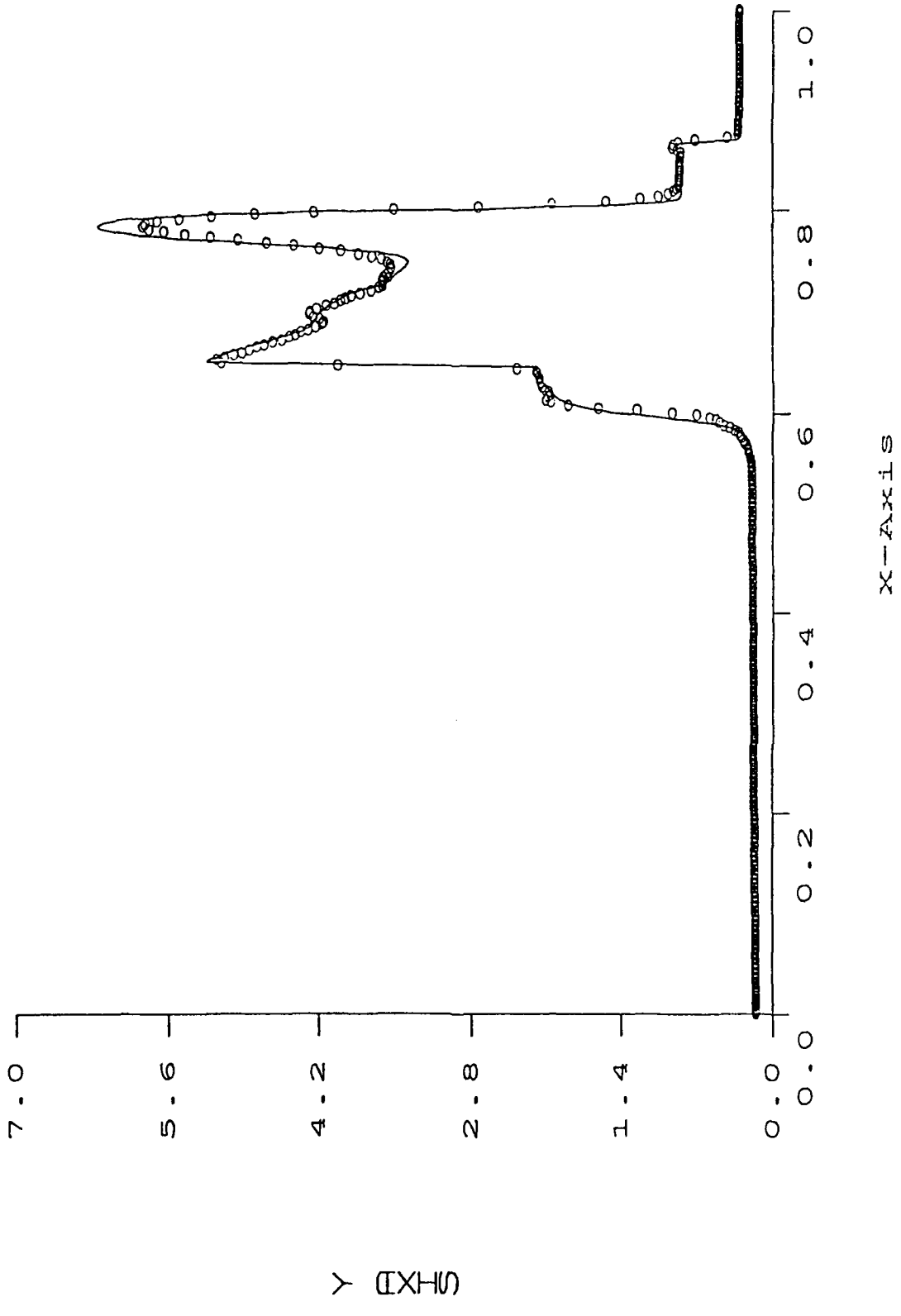

Figure 10. Blast Wave Problem with N = 400 at Time t = 0.038. (Density

Figure 11. Interactions Betwwen a Two-Dimensional Planner Shock Wave and A Vortex, Shock Mach numer = 3, t= 0.4.
(a) Density Contour with Level Value = 0.1, (b) Pressure Contour with Level Value = 0.2.

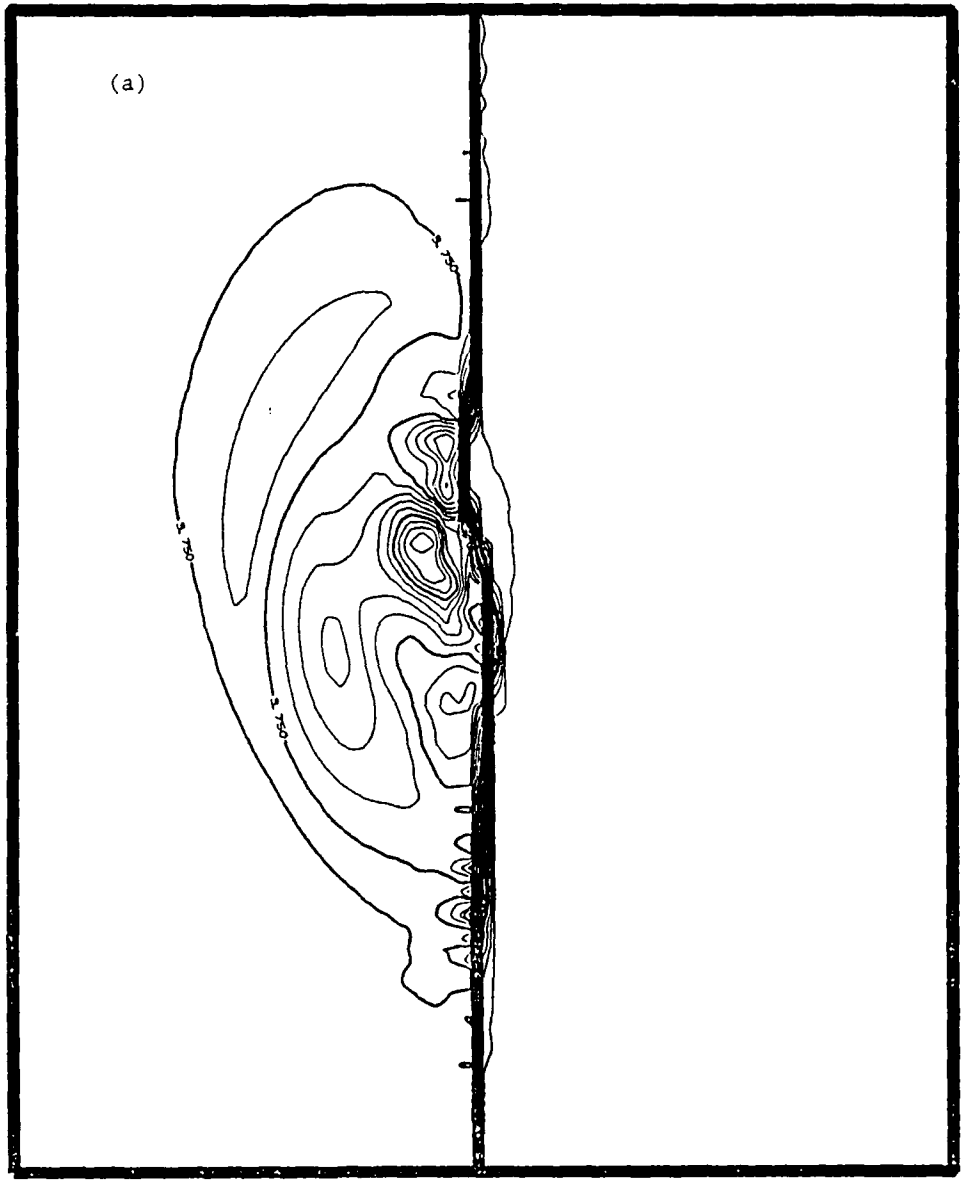

Figure 11. (Continued)

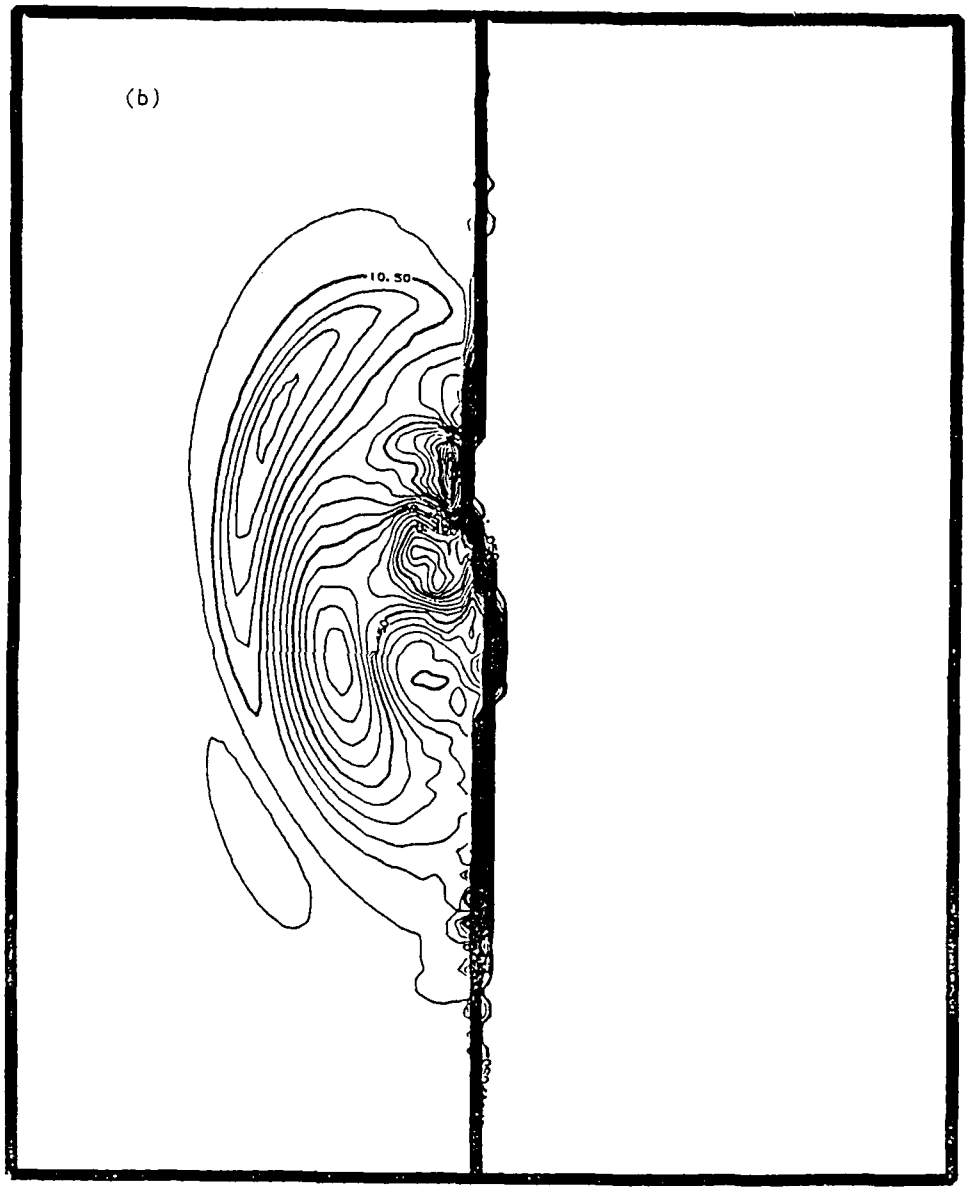

Figure 12. Close-ups of Figure 11. (a) density, (b) pressure.

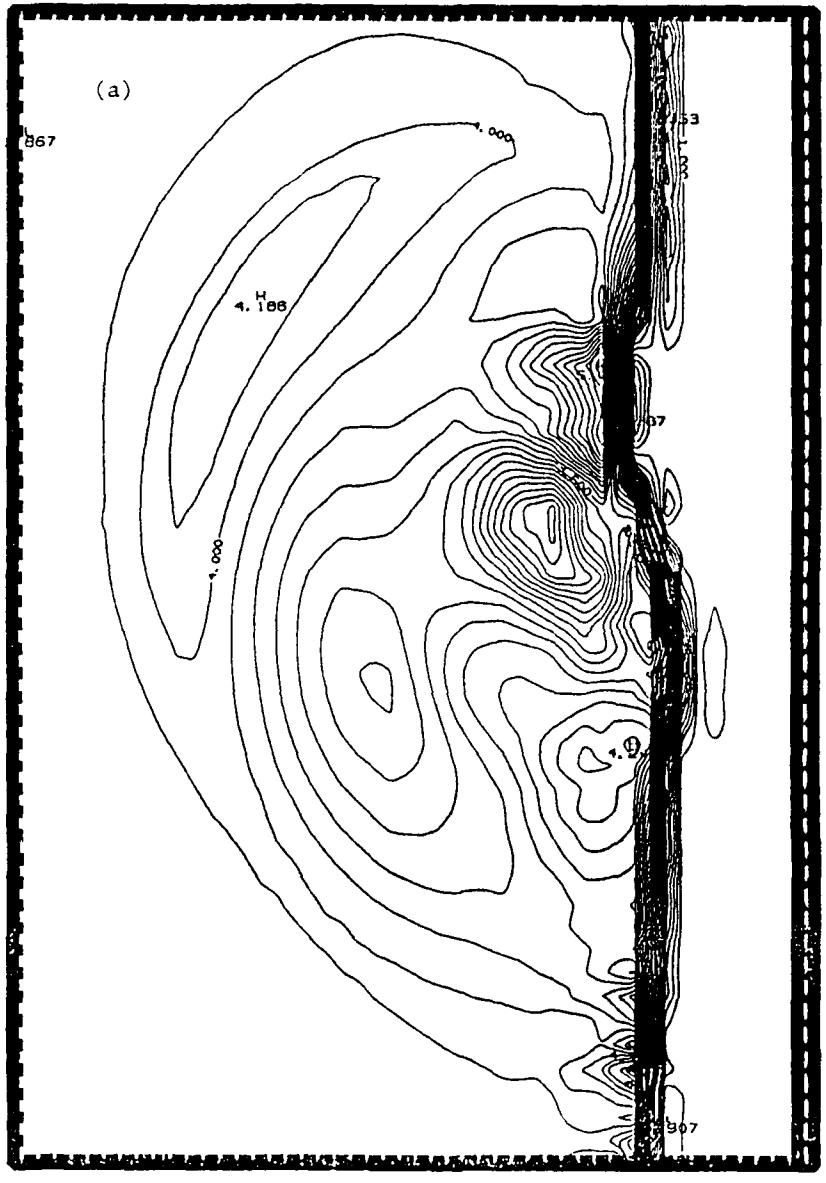

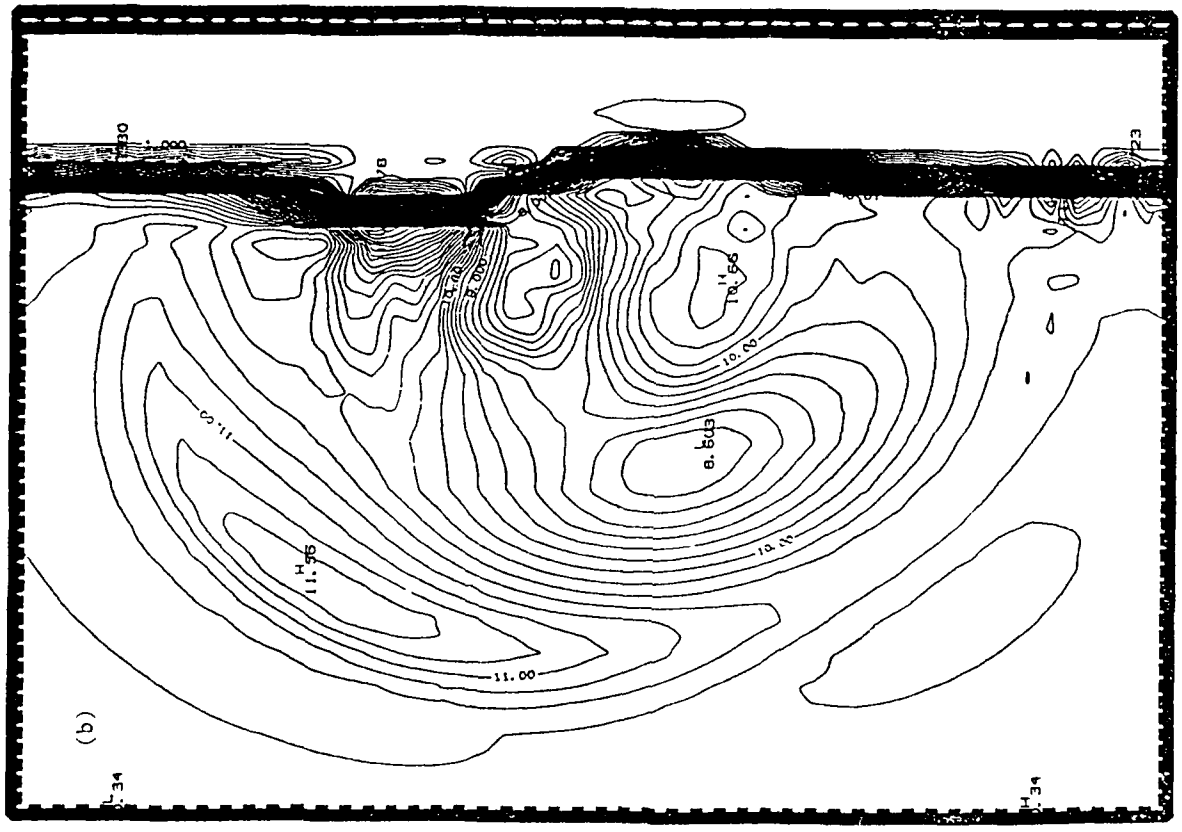

Figure 12. (Continued)

Figure 13. Same as in Figure 11, Density Solutions at Time t = 0.4.

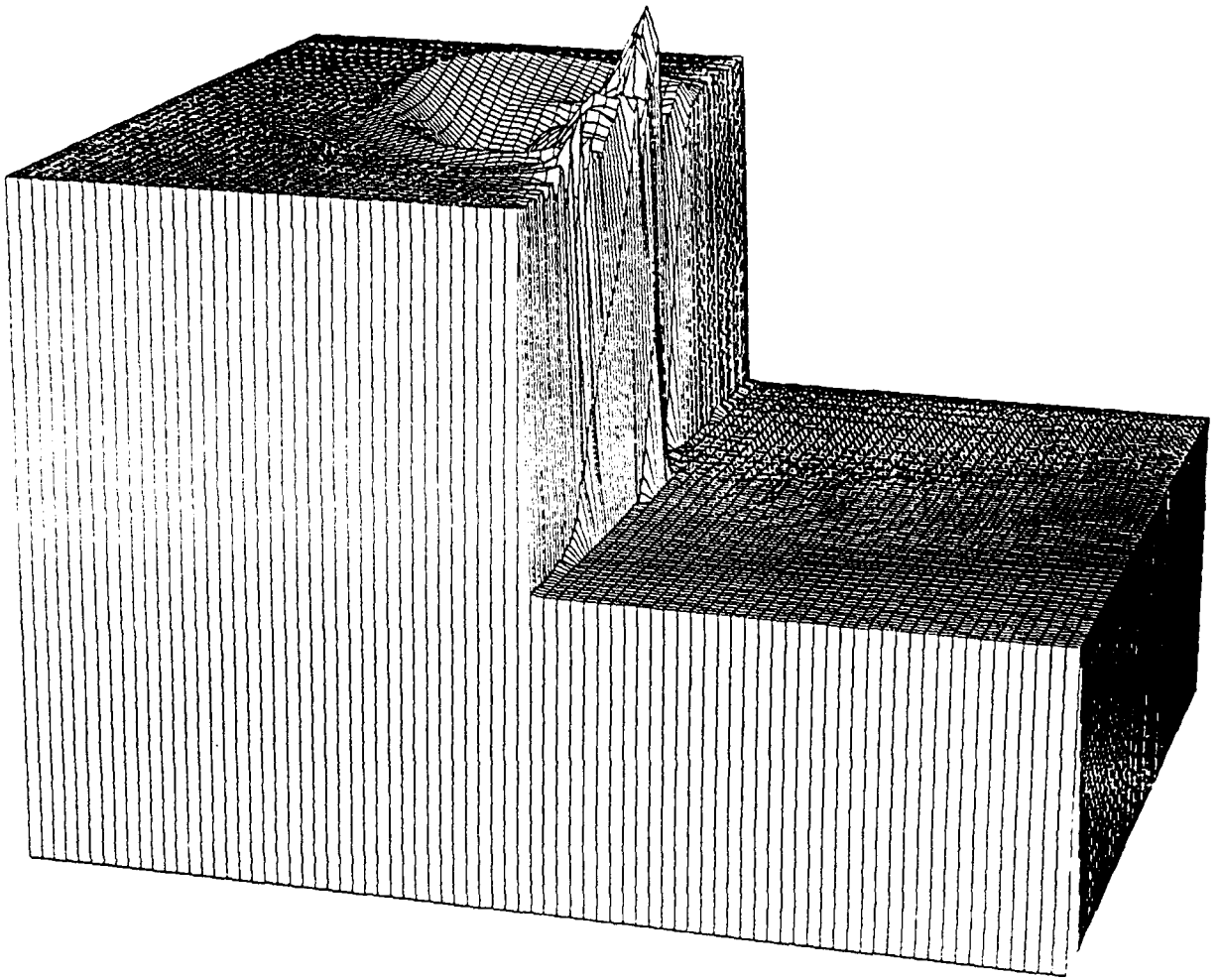

Report Documentation Page

1. Report No.	2. Government Accession No.	3. Recipient's Catalog No.
NASA CR-187535 ICASE Report No. 91-26		

4. Title and Subtitle	5. Report Date
UNIFORM HIGH ORDER SPECTRAL METHODS FOR ONE AND TWO DIMENSIONAL EULER EQUATIONS	March 1991
	6. Performing Organization Code

7. Author(s)	8. Performing Organization Report No.
Wei Cai Chi-Wang Shu	91-26
	10. Work Unit No.
	505-90-52-01
9. Performing Organization Name and Address	11. Contract or Grant No.
Institute for Computer Applications in Science and Engineering Mail Stop 132C, NASA Langley Research Center Hampton, VA 23665-5225	NAS1-18605
	13. Type of Report and Period Covered
12. Sponsoring Agency Name and Address	Contractor Report
National Aeronautics and Space Administration Langley Research Center Hampton, VA 23665-5225	14. Sponsoring Agency Code

15. Supplementary Notes

Langley Technical Monitor:
Michael F. Card

Submitted to Journal of Computational Physics

Final Report

16. Abstract

In this paper we study uniform high order spectral methods to solve multi-dimensional Euler equations for gas dynamics. Uniform high order spectral approximations with spectral accuracy in smooth regions of solutions are constructed by introducing the idea of the Essentially Non-Oscillatory (ENO) polynomial interpolations into the spectral methods. Based on the new approximations, we propose non-oscillatory spectral methods which possess the properties of both upwinding difference schemes and spectral methods. We present numerical results for the inviscid Burgers' equation, and for one dimensional Euler equations including the interactions between a shock wave and density disturbance, Sod's and Lax's shock tube problems, and the blast wave problem. Finally, we simulate the interaction between a Mach 3 two dimensional shock wave and a rotating vortex.

17. Key Words (Suggested by Author(s))	18. Distribution Statement
spectral methods, ENO finite difference methods, Conservation laws	34 - Fluid Mechanics and Heat Transfer 64 - Numerical Analysis Unclassified - Unlimited

19. Security Classif. (of this report)	20. Security Classif. (of this page)	21. No. of pages	22. Price
Unclassified	Unclassified	52	A04

NASA FORM 1626 OCT 86